Journal of Fluids and Structures (1999) **13,** 877–905
Article No.: jfls. 1999.0240, available online at http://www.idealibrary.com on IDEAL®

GUST BUFFETING AND AEROELASTIC BEHAVIOUR OF POLES AND MONOTUBULAR TOWERS

G. Solari and L.C. Pagnini

DISEG, Department of Structural and Geotechnical Engineering, University of Genova I-16145 Genova, Italy

(Received 6 November 1998 and in revised form 7 July 1999)

The evolution in the constructional field and the realization of ever more slender and light structures have emphasized the increasing difficulty of properly evaluating the actions and effects of wind on poles and monotubular towers. Faced with this situation the Italian constructors, united in a consortium coordinated by ACS ACAI Servizi, entrusted the Department of Structural and Geotechnical Engineering of Genova University with the task of formulating an *ad hoc* calculation procedure for this type of structure. This gave rise to a wide-ranging research project in which theoretical models, experimental evaluations and engineering methods were developed in parallel through an effective and quite a unique co-operation between researchers, designers and builders. This paper illustrates the physical aspects, the general principles and the basic formulation of the method proposed, with special emphasis on gust buffeting and aeroelastic phenomena. Preliminary results of full-scale measurements of the structural damping are also presented. The conclusions highlight the scientific and technical perspectives of this research.

1. INTRODUCTION

Poles and monotubular towers are generally used for lighting and telecommunication purposes. Their unit costs are limited. Their design may appear as a modest problem. The static scheme, a cantilever beam with one or more concentrated masses, is probably the simplest in the structural field. They are never excessively high.

A deeper examination of these constructions reveals completely different situations. They are built in such large numbers to represent a relevant economic problem (Figure 1). Under wind action they are subjected to dynamic effects which are seldom so complex. Independent of height, they are more slender than any other structure. The coupling of the structural slenderness with concentrated masses, especially that at the top (Figure 2), makes the problem fully aeroelastic, giving rise to potentially unstable conditions.

The consequences in the codification sector are evident. Specific standards exist (*Lighting Columns* 1985; *Public Light Poles* 1985; *Structural Standards* 1991) based on empirical calculation criteria definitely emanating from actual physical phenomena. The use of old codes, developed by considering other kinds of structures, is unjustified in this sector. The Eurocode on wind actions and effects on structures (*Basis* 1994) as well as other standards of the new generation (*Minimum Design Loads* 1995; *Technical Standards* 1996; *AIJ Recommendations* 1996) cannot be applied to these constructions. The frequent abnormal vibrations as well as some failures of poles and monotubular towers repeatedly confirmed the necessity of understanding better their wind-excited behaviour.

In an attempt to deal with this situation the ACAI (Italian Steel Constructor Association) Associates of the Poles and Monotubular Towers Section entrusted the Department of

0889–9746/99/100877 + 29 $30.00

Figure 1. Array of light poles.

Structural and Geotechnical Engineering of Genova University with the task of formulating an *ad hoc* calculation procedure for evaluating the actions and the effects of wind on this structural type. This gave rise to a wide-ranging research project where theoretical models, experimental evaluations and engineering methods were developed in parallel through an effective and quite a unique co-operation between researchers, designers and builders (Solari & Pagnini 1998; Pagnini *et al.* 1999).

This paper illustrates the theoretical basis and the analytical development of the method proposed for calculating gust buffeting and galloping effects. Starting from a general formulation involving burdensome numerical evaluations, suitable engineering simplifications are discussed and applied, leading to a solution of the problem in closed form. The solution is inspired by the procedure established by Piccardo & Solari (1998b,c) for determining the three-dimensional response of slender structures, generalizing it to the presence of localized masses and aeroelastic terms. Some results of full-scale measurements of the structural damping are also presented, highlighting the central role of this parameter. Preliminary analyses concerning the vortex shedding are discussed in another paper (Solari & Pagnini 1998).

2. WIND FIELD

Let x, y, z be a Cartesian reference system with origin at O on the ground; z is vertical and directed upwards. The wind field along z-axis is represented by the temporal law of the instantaneous $\mathbf{u}$ vectorial velocity (Figure 3):

$$\mathbf{u}(z;t) = \bar{\mathbf{u}}(z) + \mathbf{u}'(z;t), \tag{1}$$

in which t is the time, $\bar{\mathbf{u}}$ is the mean wind velocity, and $\mathbf{u}'$ is the turbulent fluctuation of $\mathbf{u}$ around $\bar{\mathbf{u}}$. Considering flat homogeneous terrains, near-neutral atmospheric conditions and the internal boundary layer, we can write

$$\bar{\mathbf{u}}(z) = \mathbf{i}\bar{u}(z), \quad \mathbf{u}'(z;t) = \mathbf{i}u'_x(z;t) + \mathbf{j}u'_y(z;t) + \mathbf{k}u'_z(z;t), \tag{2}$$

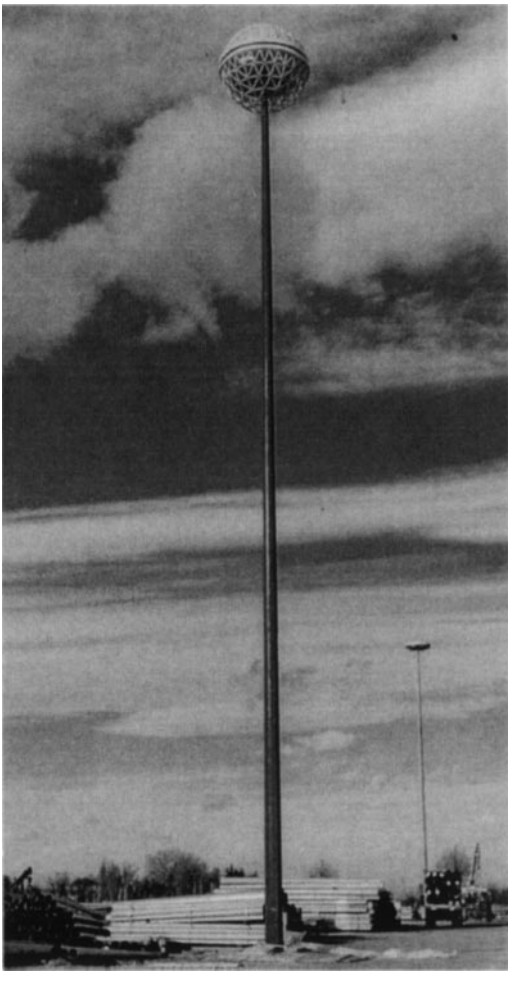

Figure 2. Monotubular light tower.

where **i**, **j**, **k** are the unit vectors associated with x, y, z; $\bar{u}$ is the mean wind velocity aligned with x; u'_x, u'_y, u'_z are the longitudinal, lateral and vertical turbulence components. As is usual in the study of vertical structures, u'_z is ignored.

The mean wind velocity profile is classically expressed by the logarithmic law (Simiu 1973)

$$\bar{u}(z) = 2{\cdot}5u_* \ln(z/z_r) \quad \text{for } z \geqslant z_m, \quad \bar{u}(z) = \bar{u}(z_m) \quad \text{for } z < z_m, \tag{3}$$

where u_* is the shear velocity, z_r is the roughness length and z_m is the value of z below which $\bar{u}$ is taken as constant to be on the safe side.

The atmospheric turbulence is a stationary Gaussian random process. It is assumed that turbulent fluctuations are small with respect to the mean wind velocity [$u'_x/\bar{u} \ll 1$, $u'_y/\bar{u} \ll 1$ (Davenport 1961)] and that u'_x and u'_y are not correlated (*Characteristics of Atmospheric Turbulence* 1993). Their cross-power spectral density functions (c.p.s.d.f.) are given by

$$S_{u_\beta u_\beta}(z, z'; n) = \sqrt{S_{u_\beta}(z; n)\, S_{u_\beta}(z'; n)}\, \mathrm{Coh}_{u_\beta u_\beta}(z, z'; n), \quad (\beta = x, y), \tag{4}$$

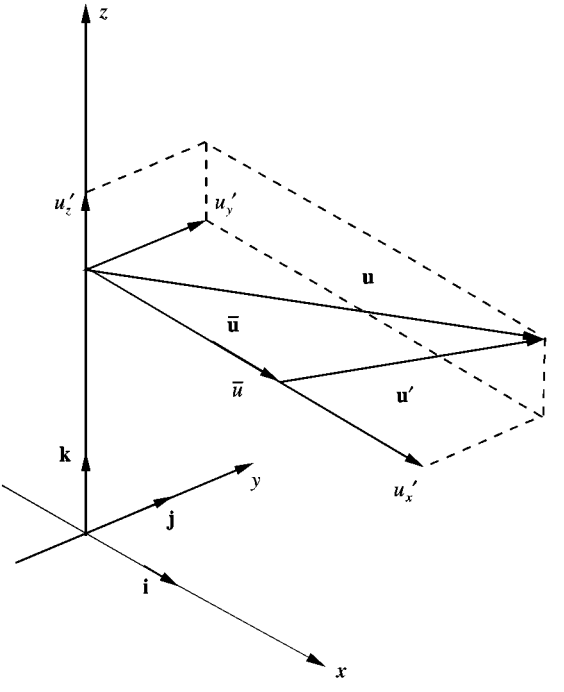

Figure 3. Wind field.

in which n is the frequency; S_{u_β} and $\mathrm{Coh}_{u_\beta u_\beta}$ are the power spectral density function (p.s.d.f.) and the coherence function of u'_β, respectively. Using the model developed by Solari & Piccardo (1999),

$$\frac{nS_{u_\beta}(z;n)}{\sigma^2_{u_\beta}} = \frac{\lambda_\beta nL_\beta(z)/\bar{u}(z)}{[1 + 1{\cdot}5\lambda_\beta nL_\beta(z)/\bar{u}(z)]^{5/3}}, \quad \mathrm{Coh}_{u_\beta u_\beta}(z, z'; n) = \exp\left\{-\frac{2nC_{z\beta}|z - z'|}{\bar{u}(z) + \bar{u}(z')}\right\}, \quad (5)$$

where $\lambda_x = 6{\cdot}868$, $\lambda_y = 9{\cdot}434$; $\sigma_{u_\beta} = I_\beta \bar{u}$ is the root-mean-square (r.m.s.) value of u'_β, assumed to be independent of height, I_β is the u'_β turbulence intensity, L_β is the integral length scale of u'_β in the x direction, and $C_{z\beta}$ is the exponential decay coefficient of u'_β along z. Suitable models of I_x, L_x, C_{zx} are given by Solari (1987) and generalized to I_y, L_y, C_{zy} by Solari & Piccardo (1999).

3. AERODYNAMIC ACTIONS

Consider the pole or the monotubular tower schematized in Figure 4. The shaft is modelled by a slender cantilever beam whose vertical axis coincides with z; its cross-section has tubular circular or polygonal shape; let h be the height of the shaft above ground; h_b is the depth of the extrados of the foundation. N localized masses are applied to the shaft — the equipment at the summit (Figure 2), the instrument or rest platforms (Figure 5) — in nodal points k ($k = 1, 2, \ldots, N$) at height z_k.

The structure undergoes aerodynamic actions partly distributed along the axis of the shaft and partly concentrated in the geometrical centre of the masses assumed as coincident with the z-axis.

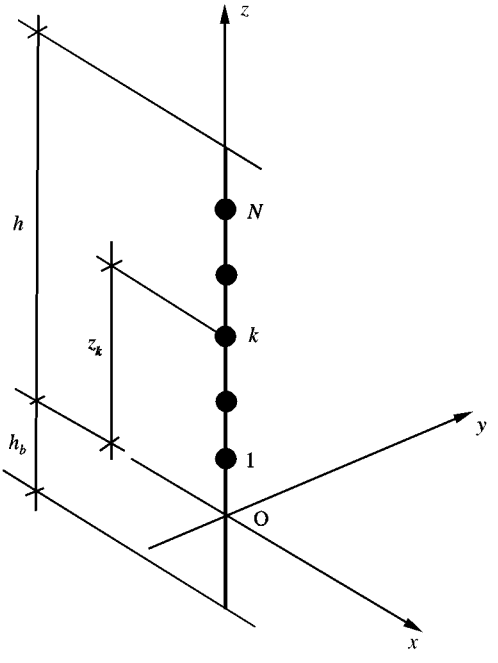

Figure 4. Structural model.

Aerodynamic actions along the shaft can be resolved into alongwind and crosswind forces F_{0x}, F_{0y}, and torsional moments M_{0z} around z. Ignoring M_{0z} due to shaft slenderness and torsional stiffness, F_{0x}, F_{0y} are given by

$$F_{0\alpha}(z;t) = \bar{F}_{0\alpha}(z) + F'_{0\alpha}(z;t), \quad (\alpha = x, y), \tag{6}$$

$\bar{F}_{0\alpha}$ being the mean value of $F_{0\alpha}$; $F'_{0\alpha}$ the fluctuation of $F_{0\alpha}$ around $\bar{F}_{0\alpha}$. Neglecting the contribution of vortex shedding, quasi-steady theory provides (Piccardo & Solari 1996)

$$\bar{F}_{0\alpha}(z) = \tfrac{1}{2}\rho\bar{u}^2(z)bc_{0\alpha x}\gamma_{\alpha x}(z), \quad F'_{0\alpha}(z;t) = \tfrac{1}{2}\rho\bar{u}(z)b\sum_{\beta} c_{0\alpha\beta}\gamma_{\alpha\beta}(z)\Xi_\beta u'_\beta(z;t), \tag{7}$$

in which ρ is the air density, b the reference size of the section, Σ_β the sum of two terms with indices $\beta = x, y$ denoting the contributions of u'_x, u'_y, respectively; $\Xi_x = 2$, $\Xi_y = 1$; $c_{0\alpha\beta}$ are the α, β elements of the matrix $[c_0]$, given by

$$[c_0] = \begin{bmatrix} c_{0xx} & c_{0xy} \\ c_{0yx} & c_{0yy} \end{bmatrix} = \begin{bmatrix} c_{0d} & c'_{0d} - c_{0l} \\ c_{0l} & c_{0d} + c'_{0l} \end{bmatrix}, \tag{8}$$

c_{0d}, c_{0l} being the drag and lift coefficients of the shaft; c'_{0d}, c'_{0l} are the prime angular derivatives of c_{0d}, c_{0l}; $\gamma_{\alpha\beta}$ is a nondimensional function by which aerodynamic properties and cross-sections varying with z are taken into account; it is called shape function and is assumed as nonnegative.

The role of vortex shedding needs further discussion. Denoting the Strouhal number by St, the shaft-shedding frequency is $n_s = \bar{u}\mathrm{St}/b$. Since b is usually small, n_s is sufficiently high to justify the use of the quasi-steady theory (Kawai 1983; Holscher & Niemann 1996)

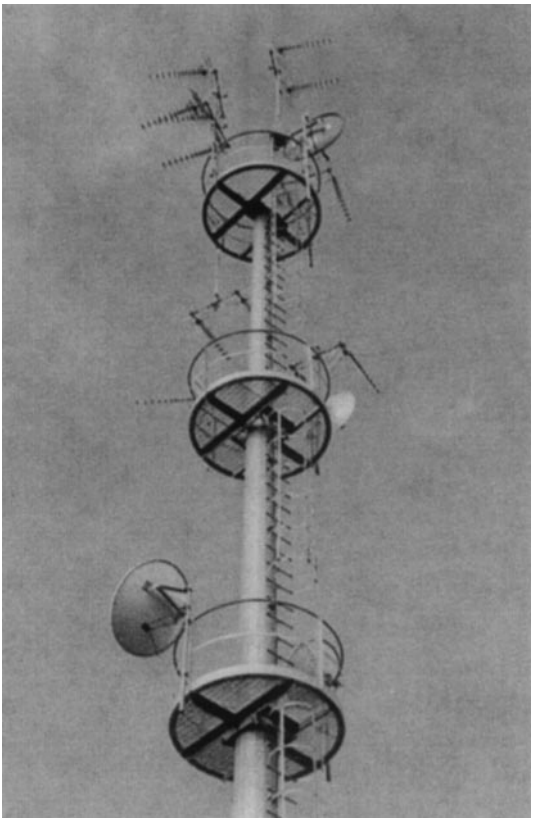

Figure 5. Monotubular tower with platforms.

especially at high design wind velocities. Moreover, it happens that the critical velocity $\bar{u}_{cr}$, i.e., the mean wind velocity which makes the vortex shedding resonant with the fundamental structural frequency, is so small as to make the quasi-static response to the wake excitation quite negligible. Critical resonant effects are singular conditions dealt with by Solari & Pagnini (1998).

Aerodynamic actions on the kth mass are represented by a force $\mathbf{F}_k$ and a moment $\mathbf{M}_k$ with Cartesian components F_{kx}, F_{ky}, F_{kz} and M_{kx}, M_{ky}, M_{kz}. Ignoring the vertical force F_{kz}, the bending moments M_{kx}, M_{ky} which are small if masses are small and compact, and the torsional moment M_{kz} which is not influential due to shaft torsional stiffness, F_{kx} and F_{ky} are given by

$$F_{k\alpha}(t) = \bar{F}_{k\alpha} + F'_{k\alpha}(t), \quad (k = 1, 2, \ldots, N), \tag{9}$$

$\bar{F}_{k\alpha}$ being the mean value of $F_{k\alpha}$, $F'_{k\alpha}$ is the fluctuation of $F_{k\alpha}$ around $\bar{F}_{k\alpha}$.

Neglecting the contribution of vortex shedding, usually irregular and with limited effects of compact isolated bluff bodies and high Reynolds numbers (Buresti 1998), $\bar{F}_{k\alpha}$, $F'_{k\alpha}$ are given by

$$\bar{F}_{k\alpha} = \tfrac{1}{2}\rho\bar{u}^2(z_k)A_k c_{k\alpha x}, \quad F'_{k\alpha}(t) = \tfrac{1}{2}\rho\bar{u}(z_k)A_k \sum_{\beta} c_{k\alpha\beta}\Xi_\beta u'_\beta(z_k; t), \tag{10}$$

where A_k is the reference size of the kth mass; $c_{k\alpha\beta}$ are the α, β elements of the matrix

$$[c_k] = \begin{bmatrix} c_{kxx} & c_{kxy} \\ c_{kyx} & c_{kyy} \end{bmatrix} = \begin{bmatrix} c_{kd} & c'_{kd} - c_{kl} \\ c_{kl} & c_{kd} + c'_{kl} \end{bmatrix} \tag{11}$$

in which c_{kd}, c_{kl} are the drag and lift coefficients of the kth mass; c'_{kd}, c'_{kl} are the first angular derivatives of c_{kd}, c_{kl}.

Combining the aerodynamic actions distributed along the shaft [equation (6)] with those applied in the localized masses [equation (9)] the global forces become

$$F_\alpha(z;t) = \bar{F}_\alpha(z) + F'_\alpha(z;t), \tag{12}$$

$$\bar{F}_\alpha(z) = \tfrac{1}{2}\rho\bar{u}^2(z)b\Gamma_{\alpha x}(z), \quad F'_\alpha(z;t) = \tfrac{1}{2}\rho\bar{u}^2(z)b\sum_\beta \Gamma_{\alpha\beta}(z)\,\Xi_\beta u'_\beta(z;t), \tag{13}$$

$$\Gamma_{\alpha\beta}(z) = c_{0\alpha\beta}\gamma_{\alpha\beta}(z) + \frac{1}{b}\sum_{k=1}^{N} A_k c_{k\alpha\beta}\,\delta(z - z_k), \tag{14}$$

where $\delta(\ \ )$ is the Dirac delta function, $\Gamma_{\alpha\beta}$ is a generalized shape function by which the composite construction dealt with in this paper can formally be treated coherently with the wind loading model proposed by Piccardo & Solari (1996) for slender structures. Since F_x, F_y are linear combinations of u'_x, u'_y, F_x, F_y are also stationary Gaussian random processes as are u'_x, u'_y. We refer to this scheme as the first level approximation. It can be simplified by analyzing the trend of the aerodynamic coefficients of the shaft and of the masses.

Figure 6 shows the coefficients c_{0d}, c_{0l} of a hexagonal element with infinite length on varying the wind direction (Hallam *et al.* 1978). There is a regular progression of c_{0d}, while c_{0l} is extremely variable. Increasing the number of sides of the polygon (poles and monotubular towers rarely have sections with less than six sides) c_{0d} is more and more regular (*Mean Fluid Forces* 1980) while c_{0l} tends to zero. In the limit case of circular section c_{0d} is constant and $c_{0l} = 0$; then $c'_{0d} = c'_{0l} = 0$. Taking also into account the fact that poles and monotubular towers usually adopt rounded corners (Figure 7), it seems reasonable to assume, for engineering purposes, $c_{0l} = c'_{0d} = 0$ independently of the shape of the polygon; $c'_{0l} = 0$ is acceptable only for regular polygons with more than eight sides (Cook 1990).

The situation is more complicated for localized masses which exhibit a wide range of complex shapes. However, since most of these are tendentially polar-symmetric (Figures 2 and 8), in this case also $c_{kl} = c'_{kd} = 0$ $(k = 1, 2, \ldots, N)$ is a reasonable engineering schematization. The further position $c'_{kl} = 0$ $(k = 1, 2, \ldots, N)$ may be applied with the exception of sharp edges (Figure 9).

Taking also into account the fact that codes often provide drag and prime derivatives of lift coefficients, while not furnishing any value of lift and prime derivatives of drag coefficients, we refer to $c_{kxy} = c_{kyx} = 0$ $(k = 0, 1, \ldots, N)$ as the second level engineering approximation. Based on this simplification the mean crosswind force [equation (13a)] is null, while F'_x, F'_y [equation (13b)] are proportional solely to u'_x, u'_y, respectively,

$$\bar{F}_y(z) = 0, \quad F'_\alpha(z;t) = \tfrac{1}{2}\rho\bar{u}(z)b\Gamma_{\alpha\alpha}(z)\Xi_\alpha u'_\alpha(z;t). \tag{15}$$

4. EQUATIONS OF MOTION AND GALLOPING CONDITIONS

Assume that the structure has a linear viscoelastic behaviour and possesses two symmetry planes intersecting along the z-axis. The line of the torsional centres coincides with z and the structure admits two sets of orthogonal modes ψ_{xi}, ψ_{yi} $(i = 1, 2, \ldots)$ belonging to planes xz,

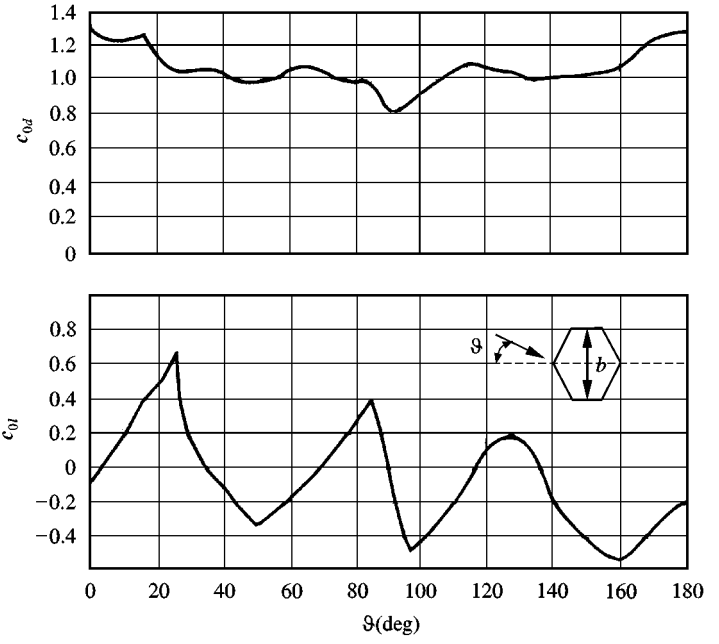

Figure 6. (a) Drag and (b) lift coefficients of a hexagonal element with infinite length [from Hallam *et al.* (1978)].

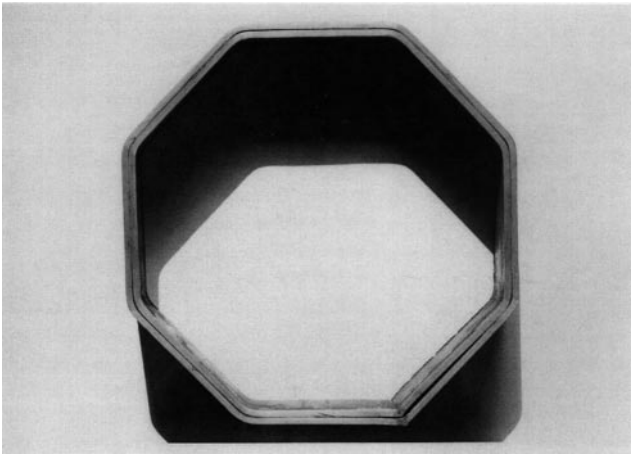

Figure 7. Cross-section of an octagonal pole.

yz, respectively. Indicating the alongwind and crosswind displacements by $\alpha = x, y$, they are given by

$$\alpha(z;t) = \sum_{i=1}^{r_\alpha} \psi_{\alpha i}(z)\, p_{\alpha i}(t), \quad p_{\alpha i}(t) = \bar{p}_{\alpha i} + p'_{\alpha i}(t), \quad (\alpha = x, y), \tag{16}$$

in which r_α is the number of modes used to reproduce the α response, $p_{\alpha i}$ is the principal coordinate associated with $\psi_{\alpha i}$, $\bar{p}_{\alpha i}$ is the mean value of $p_{\alpha i}$ and $p'_{\alpha i}$ is the fluctuation of

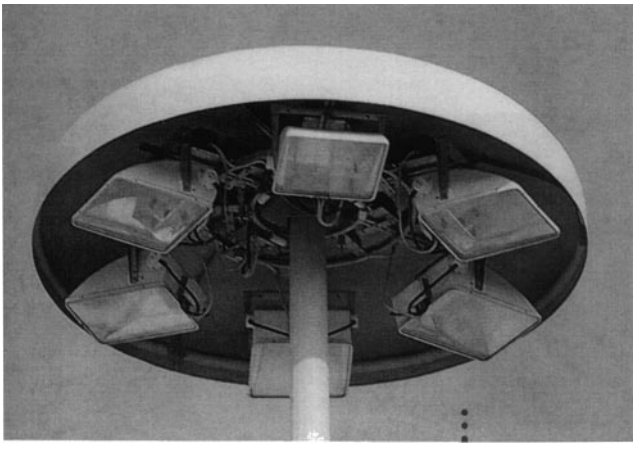

Figure 8. Typical light equipment with tendential polar symmetry.

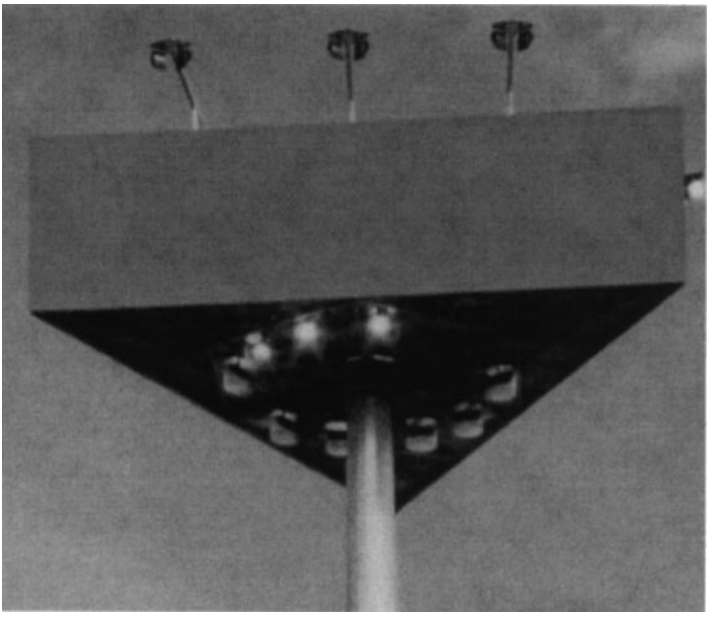

Figure 9. Special light equipment with sharp edges.

$p_{\alpha i}$ around $\bar{p}_{\alpha i}$:

$$\bar{p}_{\alpha i} = \frac{1}{(2\pi n_{\alpha i})^2} \int_0^h \bar{F}_\alpha(z)\,\psi_{\alpha i}(z)\,\mathrm{d}z \quad (i = 1, 2, \ldots, r_\alpha;\ \alpha = x, y), \tag{17}$$

$$\int_{-h_b}^h \mu(z)\,\psi_{\alpha i}(z)\,\psi_{\alpha j}(z)\,\mathrm{d}z = \delta_{ij}, \quad \mu(z) = m(z) + \sum_{k=1}^{N} M_k \delta(z - z_k), \tag{18}$$

$n_{\alpha i}$ is the ith natural frequency in plane αz, $\bar{F}_\alpha(z)$ the mean force [equation (13a)], μ the generalized mass, m the mass of the shaft per unit length, M_k the kth mass, and δ_{ij} is

Kronecker's delta. Assuming that the structural damping is proportional (Caughey 1960),

$$\ddot{p}'_{\alpha i}(t) + 2\xi_{s\alpha i}(2\pi n_{\alpha i})\,\dot{p}'_{\alpha i}(t) + (2\pi n_{\alpha i})^2\,p'_{\alpha i}(t) = \int_0^h [F'_\alpha(z;t) + \Phi'_\alpha(z;t)]\,\psi_{\alpha i}(z)\,\mathrm{d}z, \tag{19}$$

where $\xi_{s\alpha i}$ is the ith structural damping coefficient, F'_α the fluctuating aerodynamic force equation (13b), and Φ'_α the aeroelastic force due to structural motion; using the quasi-steady linearized theory [see for instance Solari (1994)], we have

$$\Phi'_\alpha(z;t) = -\tfrac{1}{2}\,\rho\bar{u}(z)\,b\sum_\beta \Gamma_{\alpha\beta}(z)\,\Xi_\beta\,\dot{\beta}(z;t), \tag{20}$$

$\sum_\beta$ being the sum of two terms with indices $\beta = x, y$, denoting the contributions of x, y, respectively. The formal analogy between equations (20) and (13b) is apparent. Substituting equation (20) into equation (19) gives

$$\begin{aligned}
&\ddot{p}'_{xi}(t) + 2\xi_{sxi}(2\pi n_{xi})\,\dot{p}'_{xi}(t) + (2\pi n_{xi})^2 p'_{xi}(t) = \int_0^h F'_x(z;t)\,\psi_{xi}(z)\,\mathrm{d}z \\
&\quad - \int_0^h \rho\bar{u}(z) b\Gamma_{xx}(z)\left[\sum_{h=1}^{r_x}\psi_{xh}(z)\,\dot{p}'_{xh}(t)\right]\psi_{xi}(z)\,\mathrm{d}z \\
&\quad - \int_0^h \tfrac{1}{2}\rho\bar{u}(z)\,b\Gamma_{xy}(z)\left[\sum_{l=1}^{r_y}\psi_{yl}(z)\,\dot{p}'_{xl}(t)\right]\psi_{xi}(z)\,\mathrm{d}z \quad (i = 1, 2, \ldots, r_x),
\end{aligned} \tag{21}$$

$$\begin{aligned}
&\ddot{p}'_{yj}(t) + 2\xi_{syj}(2\pi n_{yj})\,\dot{p}'_{yj}(t) + (2\pi n_{yj})^2 p'_{yj}(t) = \int_0^h F'_y(z;t)\,\psi_{yj}(z)\,\mathrm{d}z \\
&\quad - \int_0^h \tfrac{1}{2}\rho\bar{u}(z) b\Gamma_{yy}(z)\left[\sum_{l=1}^{r_y}\psi_{yl}(z)\,\dot{p}'_{yl}(t)\right]\psi_{yj}(z)\,\mathrm{d}z \\
&\quad - \int_0^h \rho\bar{u}(z)\,b\Gamma_{yx}(z)\left[\sum_{h=1}^{r_x}\psi_{xh}(z)\,\dot{p}'_{xh}(t)\right]\psi_{yj}(z)\,\mathrm{d}z \quad (j = 1, 2, \ldots, r_y)
\end{aligned} \tag{22}$$

which is a set of $(r_x + r_y)$ equations where aeroelastic terms have the role of coupling both x, y components of motion [through the third addenda on the right-hand sides of equations (21) and (22)] and different modes in the same plane (through the second addenda on the right-hand sides). This means that, due to aeroelasticity, the structural system becomes nonproportional (Hurty & Rubinstein 1964) and potentially unstable (Meirovitch 1980). Furthermore, the coupling of the ψ_{xi} and ψ_{yj} modes for which $n_{xi} = n_{yj}$ can give rise to unstable regimes of the bimodal galloping type (Jones 1992). This is quite relevant, since usually $n_{xi} = n_{yi}$ for all principal i coordinates.

In addition to aerodynamic actions, the equations of motion are simplified by assuming $c_{kxy} = c_{kyx} = 0 \quad (k = 0, 1, \ldots, N)$. In this case Φ'_x, Φ'_y are proportional to $\dot{x}$, $\dot{y}$ [equation (20)], respectively:

$$\Phi'_\alpha(z;t) = -\tfrac{1}{2}\,\rho\bar{u}(z)\,b\Gamma_{\alpha\alpha}(z)\,\Xi_\alpha\dot{\alpha}(z;t). \tag{23}$$

It follows that the third addenda on the right-hand sides of equations (21) and (22) vanish and the x, y components of motion become uncoupled. Nevertheless, the system retains its original coupling between different modes in the same plane which means that the initial set of $(r_x + r_y)$ equations reduces to two sets of r_x, r_y equations. They are definitely uncoupled under the condition

$$\int_0^h \bar{u}(z)\,\Gamma_{\alpha\alpha}(z)\psi_{\alpha i}(z)\psi_{\alpha j}(z)\,\mathrm{d}z = 0 \quad \text{for } i \neq j. \tag{24}$$

The literature usually regards equation (24) as an acceptable approximation if aerodynamic coefficients are positive (*Damping* 1991). The presence of negative aerodynamic coefficients does not prevent its use since the coupling of different modes at different frequencies excludes bimodal galloping (Piccardo & Luongo 1995). It follows that equations (21) and (22) become

$$\ddot{p}'_{\alpha i}(t) + 2\xi_{\alpha i}(2\pi n_{\alpha i})\,\dot{p}'_{\alpha i}(t) + (2\pi n_{\alpha i})^2\,p'_{\alpha i}(t) = \int_0^h F'_{\alpha}(z;t)\,\psi_{\alpha i}(z)\,\mathrm{d}z, \tag{25}$$

in which

$$\xi_{\alpha i} = \xi_{s\alpha i} + \xi_{a\alpha i}, \tag{26}$$

$$\xi_{a\alpha i} = \frac{\Xi_{\alpha}\rho b h \bar{u}(z_0)\psi^2_{\alpha i}(h)}{8\pi n_{\alpha i}} \sum_{k=0}^{N} c_{k\alpha\alpha} K''_{k\alpha i}, \tag{27}$$

$$K''_{0\alpha i} = \frac{\int_0^h \Delta(z)\gamma_{\alpha\alpha}(z)\psi^2_{\alpha i}(z)\,\mathrm{d}z}{h\psi^2_{\alpha i}(h)}, \quad K''_{k\alpha i} = \frac{\Delta(z_k)\,A_k\psi^2_{\alpha i}(z_k)}{bh\psi^2_{\alpha i}(h)}, \quad (k = 1, 2, \ldots, N), \tag{28}$$

$\xi_{\alpha i}$ and $\xi_{a\alpha i}$ are the ith total damping and the ith aerodynamic damping coefficients, respectively, $\Delta(z) = \bar{u}(z)/\bar{u}(z_0)$, $z_0 = 0{\cdot}6h$ is the reference height of the shaft (Solari 1982), and $K''_{k\alpha i}$ ($k = 0, 1, \ldots, N$) are nondimensional nonnegative coefficients.

Since $c_{kxx} > 0$, the alongwind aerodynamic damping is always positive. It is greater, the more light and flexible the structure is, increases with the mean wind velocity, depends on the vibration mode through the frequency and the eigenfunction value at localized mass levels.

The presence of one localized mass ($N = 1$) at the top of the shaft is the most representative case (see Figure 15). The low fundamental frequency n_{x1} and the great $\psi_{x1}(z_1)$ value cause large aerodynamic energy dissipation. Therefore, in the first mode, the mass behaves as a damper. In higher modes the increase of n_{xi} and the tendency of $\psi_{xi}(z_1)$ to become almost null reduce the aerodynamic damping to the point of making it quite negligible.

The situation changes in the crosswind direction where c_{kyy} can be negative. Classical galloping instability occurs when the total damping ξ_{yi} is null or negative, which means [equation (26)]

$$\xi_{ayi} \leq -\xi_{syi}\ (i = 1, 2, \ldots, r_y). \tag{29}$$

Since $\xi_{syi} > 0$, equation (29) may hold if a principal coordinate exists such that

$$\sum_{k=0}^{N} c_{kyy} K''_{kyi} < 0. \tag{30}$$

Equation (30) generalizes the classical Den Hartog (1932) necessary condition to this structural type. Since equation (30) is satisfied, and substituting equation (27) into (29), it is found that galloping occurs in the ith mode in plane αz when the mean wind velocity at height z_0 takes the following values:

$$\bar{u}(z_0) \geq \bar{u}_{gi} = -\frac{8\pi n_{yi}\xi_{syi}}{\rho b h \psi^2_{yi}(h)} \frac{1}{\sum_{k=0}^{N} c_{kyy} K''_{kyi}}. \tag{31}$$

If the aerodynamic coefficients depend on the mean wind velocity through the Reynolds number, equation (31) implies an iterative solution. The minimum positive value of

$\bar{u}_{gi}$ identifies the wind field producing the galloping. The case of a shaft with one mass at the top is again very meaningful.

(a) For $c_{0yy} > 0$, $c_{1yy} > 0$, the system is asymptotically stable and the crosswind aerodynamic damping increases like the alongwind aerodynamic damping (although usually of a lesser magnitude).

(b) For $c_{0yy} < 0$, $c_{1yy} > 0$, the system can gallop only if equation (30) holds. In first mode, where $\psi_{y1}(z_1)$ is large, the mass produces a relevant positive damping which counterbalances the unstable behaviour of shaft. On the other hand, since $\psi_{yi}(z_1) \approx 0$ for $i > 1$, the damping effect of the mass vanishes on higher modes and the structure tends to gallop on the second mode at $\bar{u}_{g2}$.

(c) Also for $c_{0yy} > 0$, $c_{1yy} < 0$ the system can gallop if equation (30) holds; but the large $\psi_{y1}(z_1)$ together with a negative c_{1yy} parameter gives rise to a negative damping largely exceeding the positive effect due to the shaft. Thus, the structure tends to gallop in the first mode at $\bar{u}_{g1} < \bar{u}_{g2}$.

(d) For $c_{0yy} < 0$, $c_{1yy} < 0$ equation (30) is implicitly satisfied and galloping occurs, in the first mode, at an even lower critical velocity.

5. GUST BUFFETING RESPONSE

Consider a stable system. Let $e(t)$ be any structural scalar effect (a component of the displacement, of the bending moment, of the shear force in a given direction; a local stress). It is given by

$$e(t) = \sum_{\alpha} \sum_{i=1}^{r_\alpha} \phi_{\alpha i} p_{\alpha i}(t), \tag{32}$$

$\sum_\alpha$ being the sum of two terms with indices $\alpha = x, y$, respectively, $\phi_{\alpha i}$ is the influence coefficient of $e(t)$ associated with the modal shape $\psi_{\alpha i}$. For $e(t) = \alpha\ (z; t)$, $\phi_{\beta i} = \psi_{\alpha i}(z)\delta_{\alpha\beta}$ $(\alpha, \beta = x, y)$ [equation (16)].

Due to structural linearity, e also is a stationary Gaussian random process, as are F_x, F_y. The mean maximum and minimum values of e in the period T over which wind velocity is averaged are given by (Davenport 1964)

$$\bar{e}_{\max} = \bar{e} + g_e \sigma_e, \quad \bar{e}_{\min} = \bar{e} - g_e \sigma_e, \tag{33}$$

$$g_e = \sqrt{2 \ln(\Lambda_e \nu_e T)} + \frac{0{\cdot}5772}{\sqrt{2 \ln(\Lambda_e \nu_e T)}}, \quad \nu_e = \frac{1}{2\pi} \frac{\sigma_{\dot{e}}}{\sigma_e}, \tag{34}$$

$$\sigma_e^2 = \int_0^\infty S_e(n)\, \mathrm{d}n, \quad \sigma_{\dot{e}}^2 = \int_0^\infty (2\pi n)^2 S_e(n)\, \mathrm{d}n, \tag{35}$$

where $\bar{e}$ is the mean value of e; σ_e, g_e, ν_e, S_e are respectively the r.m.s. value, the peak factor, the expected frequency and the p.s.d.f. of e', $e' = e - \bar{e}$ being the fluctuation of e around $\bar{e}$; $\sigma_{\dot{e}}$ is the r.m.s. value of $\dot{e}$; $\Lambda_e = 1$ for $\bar{e} \neq 0$, $\Lambda_e = 2$ for $\bar{e} = 0$ (Piccardo & Solari 1998b). At the first level,

$$\bar{e} = \sum_{\alpha} \sum_{i=1}^{r_\alpha} \phi_{\alpha i}\, \bar{p}_{\alpha i}, \quad S_e(n) = \sum_{\alpha} \sum_{\beta} \sum_{i=1}^{r_\alpha} \sum_{j=1}^{r_\beta} \phi_{\alpha i}\, \phi_{\beta j}\, S_{p_{\alpha i} p_{\beta j}}(n), \tag{36}$$

$\bar{p}_{\alpha i}$ being given by equation (17); $S_{p_{\alpha i} p_{\beta j}}$ is the c.p.s.d.f. of the solutions $p'_{\alpha i}(t)$, $p'_{\beta j}(t)$ of equations (21) and (22).

The situation is easier at the second level. $\bar{F}_y = 0$ [equation (15a)] implies $\bar{p}_{yj} = 0$ [equation (17)]. Since $p'_{\alpha i}(t)$, $p'_{\beta j}(t)$ are the solutions of the uncoupled equations (25),

their c.p.s.d.f. is given by

$$S_{p_{\alpha i}p_{\beta j}}(n) = H^*_{\alpha i}(n)H^*_{\beta j}(n)\int_0^h\int_0^h S_{F_\alpha F_\beta}(z, z'; n)\psi_{\alpha i}(z)\psi_{\beta j}(z')\,\mathrm{d}z\,\mathrm{d}z', \tag{37}$$

$$H_{\alpha i}(n) = \frac{1}{(2\pi n_{\alpha i})^2}\,\frac{1}{1-(n/n_{\alpha i})^2 + 2\mathrm{i}\xi_{\alpha i}\,n/n_{\alpha i}}, \tag{38}$$

where $S_{F_\alpha F_\beta}$ is the c.p.s.d.f. of F'_α, F'_β [equation (15b)]; $H_{\alpha i}$ is the complex frequency response function of the ith mode in plane αz; $H^*_{\alpha i}$ is the conjugate of $H_{\alpha i}$; i is imaginary unit. Since F'_x, F'_y are proportional to u'_x, u'_y, respectively, and u'_x, u'_y are independent, then $S_{F_\alpha F_\beta} = 0$ and $S_{p_{\alpha i}p_{\beta j}} = 0$ for $\alpha \neq \beta$; furthermore, since poles and monotubular towers have natural frequencies well separated in the same plane, $S_{p_{\alpha i}p_{\alpha j}} \approx 0$ for $i \neq j$ (Elishakoff 1983). Therefore,

$$S_e(n) = \sum_\alpha \sum_{i=1}^{r_\alpha} \phi^2_{\alpha i}\,S_{p_{\alpha i}}(n), \qquad \sigma^2_e = \sum_\alpha \sum_{i=1}^{r_\alpha} \phi^2_{\alpha i}\sigma^2_{p_{\alpha i}}, \quad \sigma^2_{\dot e} = \sum_\alpha \sum_{i=1}^{r_\alpha} \phi^2_{\alpha i}\sigma^2_{\dot p_{\alpha i}}, \tag{39}$$

where $\sigma_{p_{\alpha i}}$, $\sigma_{\dot p_{\alpha i}}$ are the r.m.s. values of $p_{\alpha i}$, $\dot p_{\alpha i}$.

The solution of the above equations calls for specific numerical approaches (Simiu & Lozier 1979; Solari 1981; *Response* 1993). Computer program DAWROS (Solari 1981), originally addressed to alongwind vibrations and now generalized to the gust-excited crosswind response, takes also into account the horizontal cross-correlation of pressure on masses of arbitrary shape. This makes the double line integral in equation (37) a quadruple integral over an articulated surface domain.

It is well recognized that the gust-excited response mainly depends on the first mode and that, at least for displacements, $r_x = r_y = 1$ usually represents an excellent approximation (Simiu & Scanlan 1996). In the present case, the potential unstable behaviour of higher modes opens the question of how wide is the neighbourhood of the bifurcation threshold where higher critical modes are significant. The example at the end of this paper and other applications not reported here demonstrate that galloping of higher modes is an "explosive" phenomenon of the critical mode in an almost vanishing neighbourhood of the bifurcation. This justifies studying the buffeting of only the first mode, provided that analyses are limited to the stable domain of the response.

6. GENERALIZED GUST FACTOR AND EQUIVALENT STATIC FORCE

Assume that the generalized displacement $\alpha = x, y$ depends only on the first modal shape $\psi_{\alpha 1}(z)$ in plane αz. Furthermore, let us define the equivalent static force $F_{\alpha\mathrm{eq}}(z)$ as the force that, applied statically in direction α, gives rise to the mean maximum displacement $\bar\alpha_{\max}(z)$. Using the method proposed by Piccardo & Solari (1996, 1998b), $\bar\alpha_{\max}$ and $F_{\alpha\mathrm{eq}}$ are given by

$$\bar\alpha_{\max}(z) = G_\alpha \bar\alpha^x(z), \quad F_{\alpha\mathrm{eq}}(z) = G_\alpha \bar F_x(z) \tag{40}$$

in which G_α is the generalized gust factor and $\bar\alpha^x$ is the static displacement caused by the application of $\bar F_x$ in the α direction. They are given by

$$G_\alpha = \frac{\bar\alpha(z)}{\bar\alpha^x(z)} + g_\alpha\,\frac{\sigma_\alpha(z)}{\bar\alpha^x(z)}, \tag{41}$$

$$\bar\alpha^x(z) = \psi_{\alpha 1}(z)\,\frac{\rho b h \bar u^2(z_0)\psi_{\alpha 1}(h)}{2(2\pi n_{\alpha 1})^2}\sum_{k=0}^{N} c_{kxx}\,\bar K_{k\alpha}, \tag{42}$$

$$\bar K_{0\alpha} = \frac{\int_0^h \Delta^2(z)\gamma_{xx}(z)\psi_{\alpha 1}(z)\,\mathrm{d}z}{h\psi_{\alpha 1}(h)}, \quad \bar K_{k\alpha} = \frac{\Delta^2(z_k)A_k\psi_{\alpha 1}(z_k)}{bh\psi_{\alpha 1}(h)}, \quad (k = 1, 2, \ldots, N), \tag{43}$$

where $\bar{K}_{k\alpha}$ ($k = 0, 1, \ldots, N$) are nondimensional nonnegative coefficients, $\bar{\alpha}$ is the mean value of α, σ_α, g_α are the r.m.s. value and the peak factor of α', $\alpha' = \alpha - \bar{\alpha}$ being the fluctuation of α around $\bar{\alpha}$; these quantities are given by equations (34)–(36) when $e(t) = \alpha(z; t)$, $r_x = r_y = 1$, $\phi_{\beta 1} = \psi_{\alpha 1}(z)\delta_{\alpha\beta}$. For $\alpha = x$ and $\bar{\alpha}^x = \bar{x}$ equations (40) and (41) identify themselves with original Davenport's formulae (1961). One has

$$\bar{\alpha}(z) = \bar{\alpha}^x(z)\delta_{\alpha x}, \quad \sigma_\alpha(z) = \bar{\alpha}^x(z)\Xi_\alpha I_\alpha(z_0)\sqrt{B_\alpha^2 + R_\alpha^2}, \quad \sigma_{\dot{\alpha}}(z) = \bar{\alpha}^x(z)\Xi_\alpha I_\alpha(z_0)(2\pi n_{\alpha 1})R_\alpha, \tag{44}$$

$$g_\alpha = \sqrt{2\ln(2\nu_\alpha T/\Xi_\alpha)} + \frac{0{\cdot}5772}{\sqrt{2\ln(2\nu_\alpha T/\Xi_\alpha)}}, \quad \nu_\alpha = n_{\alpha 1}\sqrt{\frac{R_\alpha^2}{B_\alpha^2 + R_\alpha^2}}, \tag{45}$$

$$G_\alpha = \delta_{\alpha x} + \Xi_\alpha g_\alpha I_\alpha(z_0)\sqrt{B_\alpha^2 + R_\alpha^2}, \tag{46}$$

where B_α, R_α are nondimensional coefficients associated with the background or quasi-static part and with the resonant part of the response,

$$B_\alpha^2 = \frac{(\sum_{k=0}^N c_{k\alpha\alpha}K'_{k\alpha})^2}{(\sum_{k=0}^N c_{kxx}\bar{K}_{\alpha x})^2}\int_0^\infty J_\alpha(n)\,\mathrm{d}n, \quad R_\alpha^2 = \frac{(\sum_{k=0}^N c_{k\alpha\alpha}K'_{k\alpha})^2}{(\sum_{k=0}^N c_{kxx}\bar{K}_{\alpha x})^2}\frac{\pi n_{\alpha 1}}{4\xi_{\alpha 1}}J_\alpha(n_{\alpha 1}), \tag{47}$$

$$K'_{0\alpha} = \frac{\int_0^h \Delta(z)\gamma_{\alpha\alpha}(z)\psi_{\alpha 1}(z)\,\mathrm{d}z}{h\psi_{\alpha 1}(h)}, \quad K'_{k\alpha} = \frac{\Delta(z_k)A_k\psi_{\alpha 1}(z_k)}{bh\psi_{\alpha 1}(h)}, \quad (k = 1, 2, \ldots, N), \tag{48}$$

$$J_\alpha(n) = \frac{\int_0^h\int_0^h \Delta(z)\Delta(z')\Gamma_{\alpha\alpha}(z)\Gamma_{\alpha\alpha}(z')\,S^*_{u_\alpha u_\alpha}(z, z'; n)\,\psi_{\alpha 1}(z)\psi_{\alpha 1}(z')\,\mathrm{d}z\,\mathrm{d}z'}{[\int_0^h \Delta(z)\Gamma_{\alpha\alpha}(z)\psi_{\alpha 1}(z)\,\mathrm{d}z]^2}, \tag{49}$$

where $K'_{k\alpha}$ ($k = 0, 1, \ldots, N$) are nondimensional nonnegative coefficients; $S^*_{u_\alpha u_\alpha}(z, z'; n)$ is the c.p.s.d.f. of $u^*_\alpha(z; t)$, $u^*_\alpha(z'; t)$, $u^*_\alpha = u'_\alpha/\sigma_{u_\alpha}$ being the reduced turbulence. As is typical of flexible structures, equation (45b) neglects the background part of the temporal derivative of the response (Solari 1993b).

7. CLOSED-FORM SOLUTION

The closed-form solution of the gust buffeting of poles and monotubular towers calls for the explicit expression of $\bar{K}_{0\alpha}$ [equation (43a)], $K'_{0\alpha}$ [equation (48a)], $K''_{0\alpha 1}$ [equation (28a)], B_α, R_α [equation (47)]. Noteworthy formulae of $\bar{K}_{0\alpha}$, $K'_{0\alpha}$, $K''_{0\alpha 1}$ can be obtained for given classes of $\gamma_{\alpha\alpha}$ and $\psi_{\alpha 1}$ functions (Solari & Pagnini 1998). The derivation of B_α, R_α starts from the substitution of equation (14) into equation (49):

$$J_\alpha(n) = \frac{\sum_{h=0}^N\sum_{k=0}^N c_{h\alpha\alpha}c_{k\alpha\alpha}\Omega_{hk\alpha}(n)}{(\sum_{k=0}^N c_{k\alpha\alpha}K'_{k\alpha})^2}, \tag{50}$$

where $\Omega_{00\alpha}$, $\Omega_{hk\alpha}$, $\Omega_{0k\alpha}$ ($h, k = 1, 2, \ldots, N$) are spectral contributions related to the aerodynamic actions over the shaft, to the aerodynamic cross-correlated actions over the hth and kth masses, and to the aerodynamic cross-correlated actions over the shaft and the kth mass, respectively,

$$\Omega_{00\alpha}(n) = \frac{\int_0^h\int_0^h \Delta(z)\Delta(z')\gamma_{\alpha\alpha}(z)\gamma_{\alpha\alpha}(z')\,S^*_{u_\alpha u_\alpha}(z, z'; n)\,\psi_{\alpha 1}(z)\psi_{\alpha 1}(z')\,\mathrm{d}z\,\mathrm{d}z'}{h^2\psi^2_{\alpha 1}(h)}, \tag{51}$$

$$\Omega_{hk\alpha}(n) = \frac{\Delta(z_h)\Delta(z_k)A_hA_kS^*_{u_\alpha u_\alpha}(z_h, z_k; n)\psi_{\alpha 1}(z_h)\psi_{\alpha 1}(z_k)}{b^2h^2\psi^2_{\alpha 1}(h)}, \quad (h, k = 1, 2, \ldots, N), \tag{52}$$

$$\Omega_{0k\alpha}(n) = \frac{\Delta(z_k)A_k\psi_{\alpha 1}(z_k)}{bh^2\psi^2_{\alpha 1}(h)}\int_0^h \Delta(z)\gamma_{\alpha\alpha}(z)\,S^*_{u_\alpha u_\alpha}(z, z_k; n)\,\psi_{\alpha 1}(z)\,\mathrm{d}z, \quad (k = 1, 2, \ldots, N), \tag{53}$$

The Equivalent Wind Spectrum Technique, EWST (Solari 1988) and the Generalized Equivalent Spectrum Technique, GEST (Piccardo & Solari 1998a) schematize the actual multivariate and multidimensional wind field [equations (4) and (5)] by equivalent processes identically coherent over assigned spatial domains. Using GEST, equation (51) becomes

$$\Omega_{00\alpha}(n) = K'^2_{0\alpha}\, S^*_{u_\alpha}(z_0; n)\, C\{k_{0\alpha}\eta_{0z\alpha}n\}, \tag{54}$$

where $S^*_{u_\alpha}$ is the p.s.d.f. of u^*_α, and

$$C\{\chi\} = \frac{1}{\chi} - \frac{1}{2\chi^2}\,(1 - \mathrm{e}^{-2\chi}) \quad \text{for } \chi > 0, \quad C\{0\} = 1, \tag{55}$$

$$k_{0\alpha} = \frac{1}{2}\left[\frac{1}{(h + h_b)\psi_{\alpha 1}(h)} \int_{-h_b}^{h} \psi_{\alpha 1}(z)\, \mathrm{d}z\right]^{0{\cdot}55}, \quad \eta_{0z\alpha} = \frac{\mathrm{c}_{z\alpha} h}{\bar{u}(z_0)}, \tag{56}$$

The application of EWST to equation (52) allows us to overcome the point model of masses by also considering the cross-correlation of pressure over their surface. It follows that

$$\Omega_{hk\alpha}(n) = K'_{h\alpha}K'_{k\alpha}\sqrt{S^*_{u_\alpha}(z_h; n)C\{k_{h\alpha}\eta_{hz\alpha}n\}\, C\{k_{h\alpha}\eta_{h0\alpha}n\}} \times \sqrt{S^*_{u_\alpha}(z_k; n)\, C\{k_{h\alpha}\eta_{kz\alpha}n\}\, C\{k_{k\alpha}\eta_{k0\alpha}n\}}\, \mathrm{Coh}_{u_\alpha u_\alpha}(z_h, z_k; n), \qquad (h, k = 1, 2, \ldots, N), \tag{57}$$

where

$$\eta_{k0x} = \frac{C_{yx} b_k}{\bar{u}(z_k)}, \quad \eta_{k0y} = \frac{C_{xy} \mathrm{d}_k}{\bar{u}(z_k)}, \quad \eta_{kz\alpha} = \frac{C_{z\alpha} h_k}{\bar{u}(z_k)}, \quad (k = 1, 2, \ldots, N), \tag{58}$$

$k_{k\alpha} = 0{\cdot}4\ (k = 1, 2, \cdots, N)$; $C_{\alpha\beta}$ is the exponential decay coefficient of u'_β in direction α; d_k, b_k, h_k $(k = 1, 2, \ldots, N)$ are the reference sizes of the kth mass parallel to x, y, z, respectively.

The development of equation (53) calls for the joint use of EWST, GEST and some further numerical evaluations. This mixed approach leads to the relationship

$$\Omega_{0k\alpha}(n) \approx K'_{0\alpha}K'_{k\alpha}\sqrt{S^*_{u_z}(z_0; n)\, C\{k_{0\alpha}\eta_{0z\alpha}n\}} \times \sqrt{S^*_{u_\alpha}(z_k; n)\, C\{k_{k\alpha}\eta_{kz\alpha}n\}\, C\{k_{k\alpha}\eta_{k0\alpha}n\}}\, \mathrm{Coh}_{u_\alpha u_\alpha}(z_0, z_k; \theta n), \quad (k = 1, 2, \ldots, N), \tag{59}$$

where θ is a nondimensional coefficient in the range [0,1]. For $\theta = 0$ (unit coherence) and 1 (actual coherence) equation (59) tends to overestimate and underestimate $\Omega_{0k\alpha}$, respectively; $\theta = 0{\cdot}5$ (square root of the coherence) represents a suitable average choice.

Substituting equations (54), (57) and (59) into equation (50) and equation (50) into equation (47b) provides

$$R^2_\alpha = \frac{1}{\left(\sum_{k=0}^{N} c_{kxx}\, \bar{K}_{k\alpha}\right)^2} \sum_{h=0}^{N}\sum_{k=0}^{N} c_{h\alpha\alpha}\, c_{k\alpha\alpha} K'_{h\alpha}K'_{k\alpha} R_{h\alpha}R_{k\alpha}\, \mathrm{Coh}_{u_\alpha u_\alpha}(z_h, z_k; \theta_{hk} n_{\alpha 1}), \tag{60}$$

where $\theta_{h0} = \theta_{0k} = 0{\cdot}5$ for $h, k > 0$; $\theta_{hk} = 1$ in all other cases. $R_{0\alpha}$, $R_{k\alpha}$ $(k = 1, 2, \ldots, N)$ are the parts of the resonant contribution R_α associated, respectively, with the shaft and the kth mass:

$$R^2_{0\alpha} = \frac{\pi}{4\xi_{\alpha 1}} \frac{\lambda_x \tilde{n}_{0\alpha}}{(1 + 1{\cdot}5\lambda_x \tilde{n}_{0\alpha})^{5/3}}\, C\{\tilde{n}_{0\alpha}\tilde{h}_{0\alpha}\}, \tag{61}$$

$$R^2_{k\alpha} = \frac{\pi}{4\xi_{\alpha 1}} \frac{\lambda_x \tilde{n}_{k\alpha}}{(1 + 1{\cdot}5\lambda_x \tilde{n}_{k\alpha})^{5/3}}\, C\{\tilde{n}_{k\alpha}\tilde{h}_{k\alpha}\}\, C\{\tilde{n}_{k\alpha}\tilde{w}_{k\alpha}\}, \quad (k = 1, 2, \ldots, N), \tag{62}$$

where, putting $h_0 = h$,

$$\tilde{h}_{k\alpha} = \frac{k_{k\alpha}\lambda_x C_{z\alpha} h_k}{\lambda_\alpha L_\alpha(z_k)}, \quad \tilde{n}_{k\alpha} = \frac{n_{\alpha 1}\lambda_\alpha L_\alpha(z_k)}{\lambda_x \bar{u}(z_k)}, \quad (k = 0, 1, \ldots, N), \tag{63}$$

$$\tilde{w}_{kx} = \frac{k_{kx} C_{yx} b_k}{L_x(z_k)}, \quad \tilde{w}_{ky} = \frac{k_{ky}\lambda_x C_{xy} d_k}{\lambda_y L_y(z_k)}, \quad (k = 1, 2, \ldots, N). \tag{64}$$

The analytical evaluation of the background response may be obtained by substituting equations (54), (57) and (59) into equation (50), and equation (50) into equation (47a), having set $\mathrm{Coh}_{u_\alpha u_\alpha}(z, z'; n) = \mathrm{Coh}_{u_\alpha u_\alpha}(z, z'; n_{\alpha m})$, where $n_{\alpha m}$ is an average frequency of the p.s.d.f. of u'_α assumed as representative of the harmonic content of the background part of the response. Since $n_{\alpha m} \ll n_{\alpha 1}$, $\mathrm{Coh}_{u_\alpha u_\alpha}(z, z'; n_{\alpha m}) \approx 1$ applies. Generalizing equation (60) to B^2_α, equation (47a) may be approximated by the formula

$$B^2_\alpha = \frac{(\sum_{k=0}^{N} c_{k\alpha\alpha} K'_{k\alpha} B_{k\alpha})^2}{(\sum_{k=0}^{N} c_{kxx} \bar{K}_{k\alpha})^2}, \tag{65}$$

which provides reliable estimates especially for $N = 1$. $B_{0\alpha}$, $B_{k\alpha}$ $(k = 1, 2, \ldots, N)$ are the parts of the background contribution B_α associated, respectively, with the shaft and the kth mass; using the closed-form solutions developed by Solari (1982, 1993a, b) and Piccardo & Solari (1998b, c),

$$B^2_{0\alpha} = \frac{1}{1 + 0{\cdot}30\tilde{h}^{0{\cdot}63}_{0\alpha}}, \quad B^2_{k\alpha} = \frac{1}{1 + 0{\cdot}334(\tilde{h}_{k\alpha} + \tilde{w}_{k\alpha})^{0{\cdot}63}}, \quad (k = 1, 2, \ldots, N). \tag{66}$$

Equations (60) and (65) point out the relative roles of the shaft and of the masses. With the surface of the masses tending to zero, the structure tends to the classical slender cantilever vertical beam. In the dual case in which there is one mass of dominant size on the remaining surface, the point-like model is realized (Solari 1982). The closed formulae obtained by Solari (1993a, b) and by Piccardo & Solari (1998b, c) can be regarded as particular cases of the above solution.

Finally, it is important to stress the case in which not all coefficients c_{kyy} $(k = 0, 1, \ldots, N)$ have the same sign. If this involves a relevant response over the modes higher than the first, the gust factor technique cannot be applied and a numerical approach (Section 5) has to be used.

8. COMBINATION RULES

The closed-form solution allows one to determine $\bar{p}_{\alpha 1}$, $\sigma_{p_{\alpha 1}}$, $\sigma_{\dot{p}_{\alpha 1}}$ by dividing $\bar{\alpha}$, σ_α, $\sigma_{\dot{\alpha}}$ [equation (44)] by $\psi_{\alpha 1}$. The further use of the second level approach provides the mean maximum and minimum values of a generic scalar effect $e(t)$ [equations (33)–(35)], assuming p_{x1}, p_{y1} as independent. Even though theory proves this assumption, experience has shown many cases in which alongwind and crosswind responses are partially correlated (Ballio & Solari 1992; Holmes *et al.* 1992). The combination rule proposed by Solari *et al.* (1998) takes this fact into account, becoming very expressive if jointly applied together with the gust factor technique.

Let $\boldsymbol{\omega}(t)$ be a vectorial effect (a displacement, a bending moment or a shear force) given by

$$\boldsymbol{\omega}(t) = \mathbf{i}\omega_x(t) + \mathbf{j}\omega_y(t), \tag{67}$$

where ω_α is the component of $\boldsymbol{\omega}$ due to the α response $(\alpha = x, y)$; since $\bar{y} = 0$, also $\bar{\omega}_y = 0$. Let $\bar{\omega}_{\alpha\max}$ be the mean maximum value of ω_α; $\bar{\omega}_{\max}$ is the mean maximum value of the Euclidean norm ω of $\boldsymbol{\omega}$. The probability that ω exceeds $\bar{\omega}_{\max}$ is defined as *small*.

If ω_x, ω_y are noncorrelated processes, the probability that ω crosses the eliptical threshold in Figure 10 is small, and $\bar{\omega}_{\max} \approx \max\{\bar{\omega}_{x\max}, \bar{\omega}_{y\max}\}$. In the dual case in which ω_x, ω_y are perfectly positively or negatively correlated, ω lies, with small probability of going outside, on the BD or AC diagonals of the rectangle ABCD, and $\bar{\omega}^2_{\max} \approx \bar{\omega}^2_{x\max} + \bar{\omega}^2_{y\max}$.

Defining the probability that ω exceeds the polygonal threshold $P_1, P_2, \ldots, P_{12}$ as small, $\bar{\omega}_{\max}$ is the length of the vector joining the origin of plane ω_x, ω_y with the most distant point of the polygon;

$$\bar{\omega}_{\max} = \max\{\omega_1, \omega_2, \ldots, \omega_{12}\}, \tag{68}$$

$$\omega_l = \sqrt{[\bar{\omega}^x_x(1 - a_{xl} + a_{xl}G_x)]^2 + [\bar{\omega}^x_y a_{yl} G_y]^2}, \quad (l = 1, 2, \ldots, 12), \tag{69}$$

where $\bar{\omega}^x_\alpha$ is the ω_α value caused by the application of $\bar{F}_x$ in direction α; $a_{\alpha l}$ are nondimensional coefficients listed in Table 1 where $\eta = 0{\cdot}3$, $\gamma = 0{\cdot}8$ [Figure 10; Solari *et al.* (1998)].

The 12 combination rules defined by equation (69) correspond to the application of the following 12 loading conditions:

$$F_{x\mathrm{eq},l}(z) = (1 - a_{xl} + a_{xl}G_x)\bar{F}_x(z) \cup F_{y\mathrm{eq},l}(z) = a_{yl}G_y\bar{F}_x(z), \quad (l = 1, 2, \ldots, 12) \tag{70}$$

in which $\cup$ is the union symbol (simultaneous application).

Consider the scalar effect $e(t)$ already studied in Section 4 and assume

$$e(t) = \kappa_x\omega_x(t) + \kappa_y\omega_y(t), \tag{71}$$

where κ_x, κ_y are influence coefficients. Due to equations (68)–(70), equation (33) becomes

$$\bar{e}_{\max} = \max\{e_1, e_2, \ldots, e_{12}\}, \quad \bar{e}_{\min} = \min\{e_1, e_2, \ldots, e_{12}\}, \tag{72}$$

$$e_l = \kappa_x\bar{\omega}^x_x(1 - a_{xl} + a_{xl}G_x) + \kappa_y\bar{\omega}^x_y a_{yl}G_y, \quad (l = 1, 2, \ldots, 12). \tag{73}$$

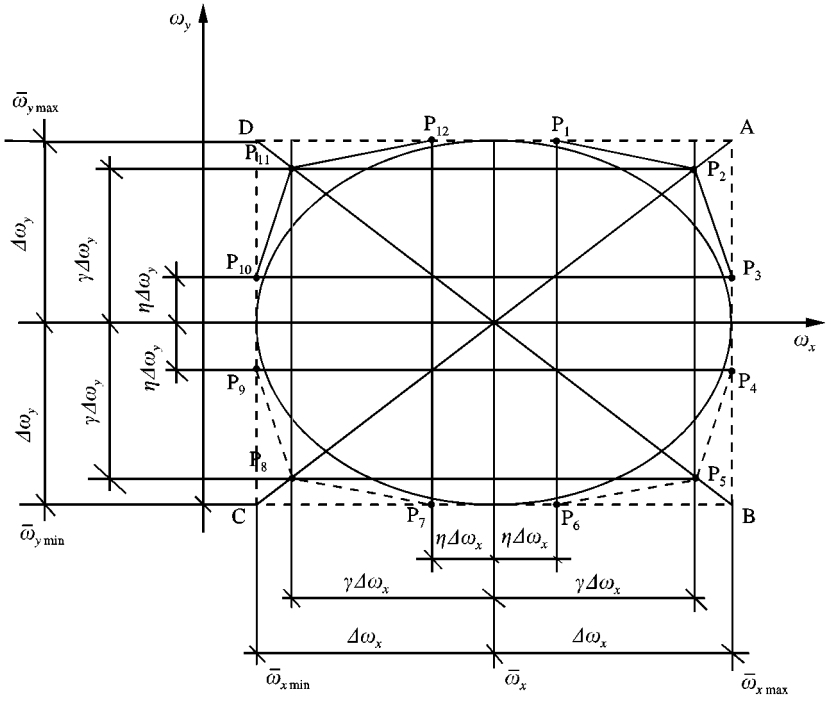

Figure 10. Combination rule for vectorial effects.

In contrast to equation (33), equations (72) and (73) involve only analytical evaluations and, moreover, minimize the risk of underestimating the effect.

9. FULL-SCALE MEASUREMENTS

The procedure described in the foregoing highlights the central role of the structural damping especially in proximity to galloping instability. An analogous role of the structural damping is apparently close to the resonant shedding conditions (Solari & Pagnini 1998). Faced by the necessity of correctly evaluating this quantity, the literature has little reliable data. Eurocode 1, for instance, gives semi-empirical values of the structural damping of generic steel elements. Specific studies on poles and monotubular towers (Yam *et al.* 1997) are almost totally lacking.

In order to overcome this limitation, full-scale experiments were carried out by Pagnini *et al.* (1999) on five sample structures. Free damped vibrations were induced by pulling and releasing a cable. The cable was pulled by jacks. The release was obtained by interposing steel test pieces or nylon wires between the shaft and the cable (Figure 11). The section of the test pieces and the number of wires were chosen to break in correspondence with preordained displacements. The tests were repeated for each sample structure, varying both the position of the cable and the imposed displacement.

TABLE 1

Parameters a_{xl}, a_{yl} for $l = 1, 2, \ldots, 12$

l	1	2	3	4	5	6	7	8	9	10	11	12
a_{xl}	η	γ	1	1	γ	η	$-\eta$	$-\gamma$	-1	-1	$-\gamma$	$-\eta$
a_{yl}	1	γ	η	$-\eta$	$-\gamma$	-1	-1	$-\gamma$	$-\eta$	η	γ	1

Figure 11. Apparatus for releasing the cable.

Structures were monitored by accelerometers (Figure 12). Displacements were obtained by integrating the accelerations, using suitable harmonic filters to circumscribe the oscillations decaying in selected modes. Structural damping coefficients were derived by considering temporal segments of the displacement with different values of the motion amplitude.

Some further results were available from previous full-scale experiments carried out by Solari (1992) on an urban light pole excited by a vibrodyne.

Figure 13 summarizes the main results of the experiments (Pagnini *et al*. 1999), showing the first structural damping coefficient as a function of top displacement. Although the structural sample is not sufficient to allow statistical evaluations, it is apparent that damping increases while increasing the motion amplitude, according to laws depending on the type of structure. Eurocode gives damping values on the safe side.

10. NUMERICAL APPLICATION

To show and discuss some typical results of the calculation method, let us examine the urban light pole previously subjected to full-scale experiments by Solari (1992) and analyzed by Solari & Pagnini (1998). The shaft has an octagonal conical shape and is made of steel sheeting with constant thickness. There is one light equipment at the summit ($N = 1$). Table 2 summarizes the main geometric and structural properties.

Figure 14(a–e) shows a schematic of the pole, the thickness s, the diameter ϕ of circumscribed circumference, the area A and the moment of inertia J of the cross-section of

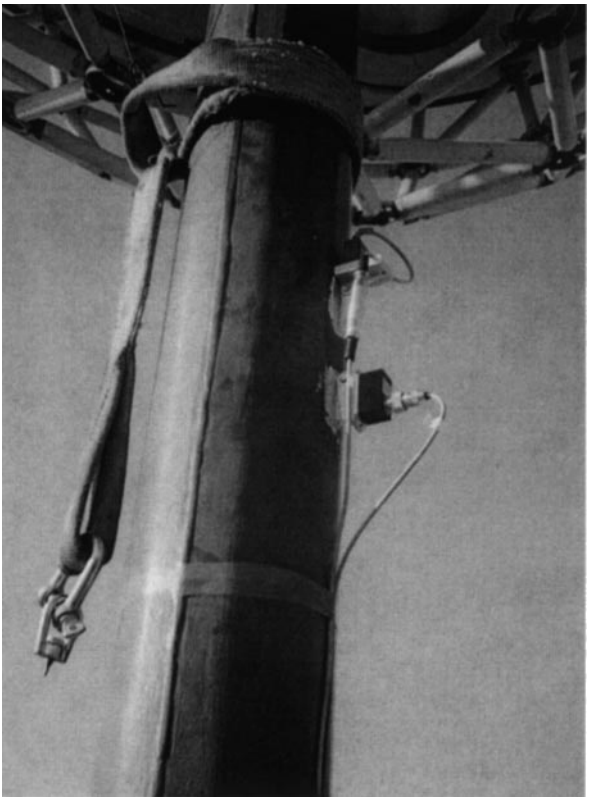

Figure 12. Accelerometer at the top of the shaft.

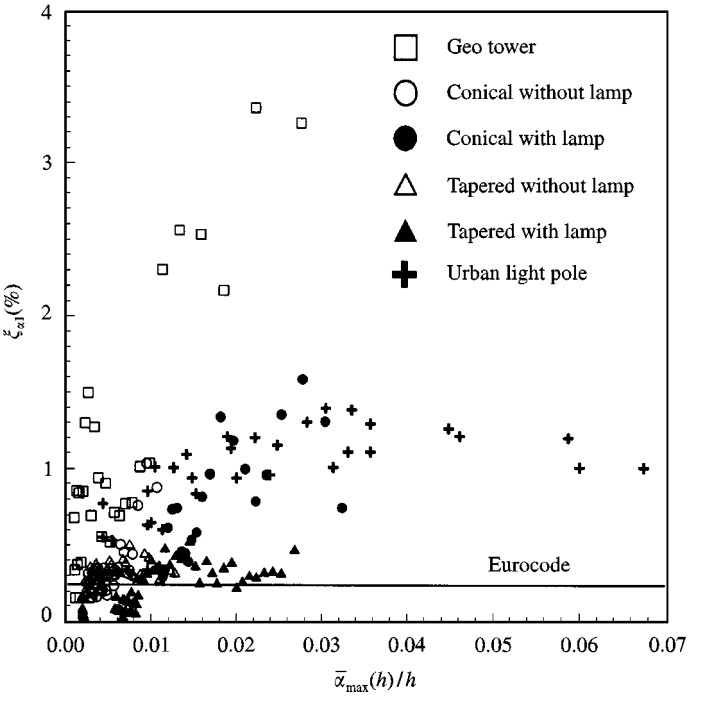

Figure 13. First structural damping coefficient versus motion amplitude.

TABLE 2

Geometric and structural properties

Shaft	Steel-sheeting thickness	$s = 4$ mm
	Height above ground	$h = 14$ m
	Depth of foundation extrados	$h_b = 0$
	Outer base diameter	$\phi_b = 280$ mm
	Outer top diameter	$\phi_1 = 80$ mm
Equipment	Mass	$M_1 = 145$ kg
	Height of barycentre	$z_1 = 14{\cdot}9$ m

the shaft. Figure 14 (f–h) shows the modes $\psi_{\alpha i}$ ($\alpha = x, y$); $\psi_{\alpha i}(z_1) = \psi_{\alpha i}(h) + (z_1 - h)\,\psi'_{\alpha i}(h)$, where $\psi'_{\alpha i}$ is the first derivative of $\psi_{\alpha i}$ with respect to z. Table 3 lists the natural frequencies $n_{\alpha i}$, $\psi_{\alpha i}(h)$ and $\psi_{\alpha i}(z_1)$.

The structure stands in homogeneous terrain with $z_r = 0{\cdot}1$ and $z_m = 5$ m. Table 4 summarizes the properties of atmospheric turbulence. The shear velocity u_* varies between 0 and 4 m/s.

Table 5 provides the main aerodynamic properties of shaft and equipment. The drag coefficient of the shaft depends on Reynolds number $\mathrm{Re} = \phi\bar{u}/\nu$, where $\nu = 15 \times 10^{-6}$ m^2/s is the kinematic viscosity of the air; for $2{\cdot}4 \times 10^5 \leq \mathrm{Re} \leq 3 \times 10^5$, c_{0d} is obtained through logarithmic interpolation. The drag coefficient of the mass is independent of Reynolds number. On varying the wind direction $c_{0yy} = (c_{0d} + c'_{0l})$ takes on values between -1 and 1 while $c_{1yy} = (c_{1d} + c'_{1l})$ is between $-0{\cdot}3$ and $0{\cdot}3$. There are consequently four possible

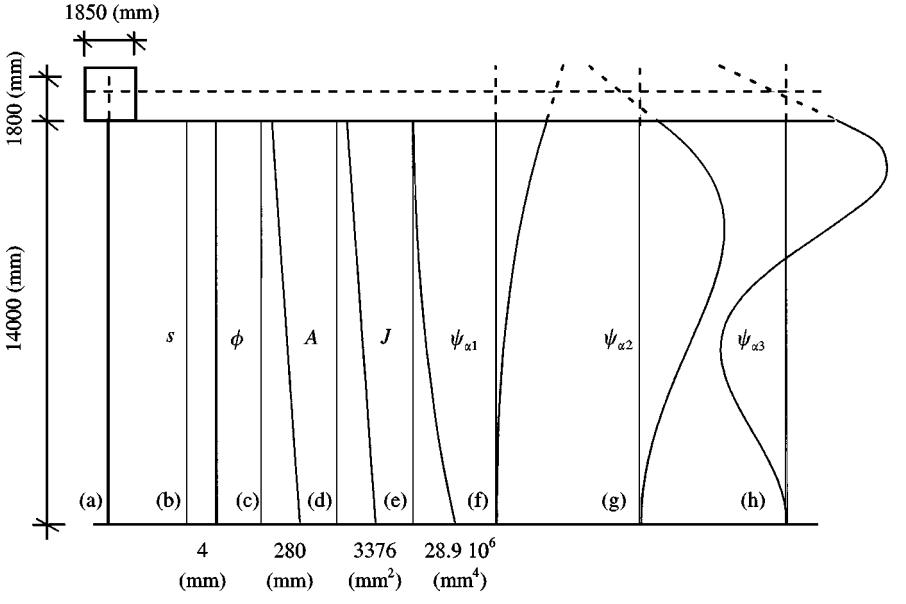

Figure 14. (a) Schematic diagram of the sample structure; (b) sheet thickness; (c) outer diameter; (d) cross-sectional area; (e) moment of inertia; (f–h) first three modes.

TABLE 3

Natural frequencies and mode shape values ($\alpha = x, y$)

Mode i	$n_{\alpha i}$ (Hz)	$\psi_{\alpha i}$ (h)	$\psi_{\alpha i}$ (z_1)
1	0·549	0·0676	0·0784
2	3·597	0·0216	− 0·0230
3	10·287	0·0650	− 0·0115

TABLE 4

Atmospheric turbulence properties

Turbulence intensities	$I_x(z) = 1/\ln(z/z_r)$
	$I_y(z) = 0{\cdot}78\ I_x(z)$
Integral length scales	$L_x(z) = 300\ (z/300)^{0{\cdot}29}$ (L_x, z in m)
	$L_y(z) = 0{\cdot}25\ L_x(z)$
Exponential decay coefficients	$C_{yx} = C_{zx} = 11{\cdot}5\ C_{zy} = 7$
	$C_{xy} = 0$ (on the safe side)

aerodynamic configurations denoted by A,B,C,D as summarized in Table 6. Coherently with the second level approach, $c_{0xy} = c_{0yx} = c_{1xy} = c_{1yx} = 0$.

Assuming conventionally that the structural damping is $\xi_{s\alpha i} = 0{\cdot}004775$ ($2\pi\xi_{s\alpha i} = 0{\cdot}03$) for all modes (Solari & Pagnini 1998), Figures 15 and 16 show the diagrams of ξ_{xi} and ξ_{yi} [equation (26)] in terms of u_*. By the virtue of the mass at the top, the first alongwind aerodynamic damping (Figure 15) largely exceeds the structural part in the design wind

TABLE 5

Main aerodynamic properties

Shaft	Reference height	$z_0 = 0{\cdot}6h = 8{\cdot}4\ m$
	Reference size	$b = \phi\ (z_0) = 0{\cdot}16\ m$
	Drag coefficient	$c_{0d} = 1{\cdot}334$ for $\mathrm{Re} \leq 2{\cdot}4 \times 10^5$
		$c_{0d} = 1{\cdot}196$ for $\mathrm{Re} \geq 3 \times 10^5$
Mass	Reference height	$h_1 = 1{\cdot}80$ m
	Reference size	$b_1 = 1{\cdot}85$ m
	Reference area	$A_1 = b_1 h_1 = 3{\cdot}33\ \mathrm{m}^2$
	Drag coefficient	$c_{1d} = 0{\cdot}3$

TABLE 6

Basic aerodynamic configurations

Case	c_{oyy}	c_{1yy}
A	1	0·3
B	− 1	0·3
C	1	− 0·3
D	− 1	− 0·3

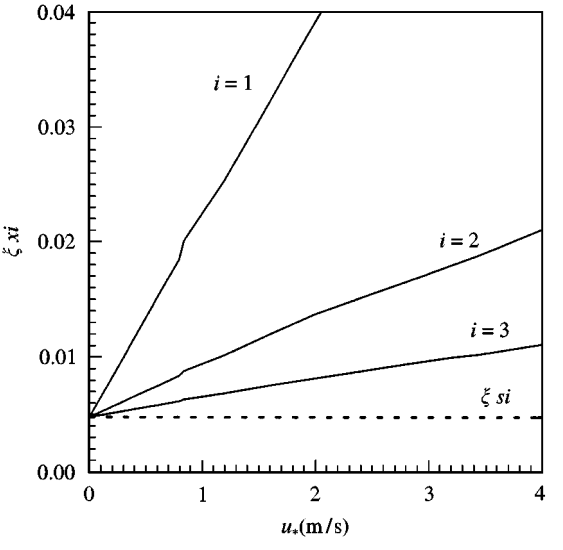

Figure 15. Damping coefficient in the alongwind direction.

velocity range. The crosswind aerodynamic damping (Figure 16) follows the tendency discussed in Section 4. In case A, ξ_{yi} is positive and the response is always asymptotically stable. In case B, the galloping of the second mode is realized when $u_* = 3{\cdot}606$ m/s (shaded domain). In case C, the galloping involves the second mode at $u_* = 0{\cdot}843$ m/s. Case D, somewhat improbable, gives rise to the galloping of the first mode for $u_* = 0{\cdot}586$ m/s.

Figure 17 shows the diagrams of the generalized gust factor G_α ($\alpha = x, y$). Solid lines correspond to the solution provided by DAWROS (Solari 1981), taking the first three

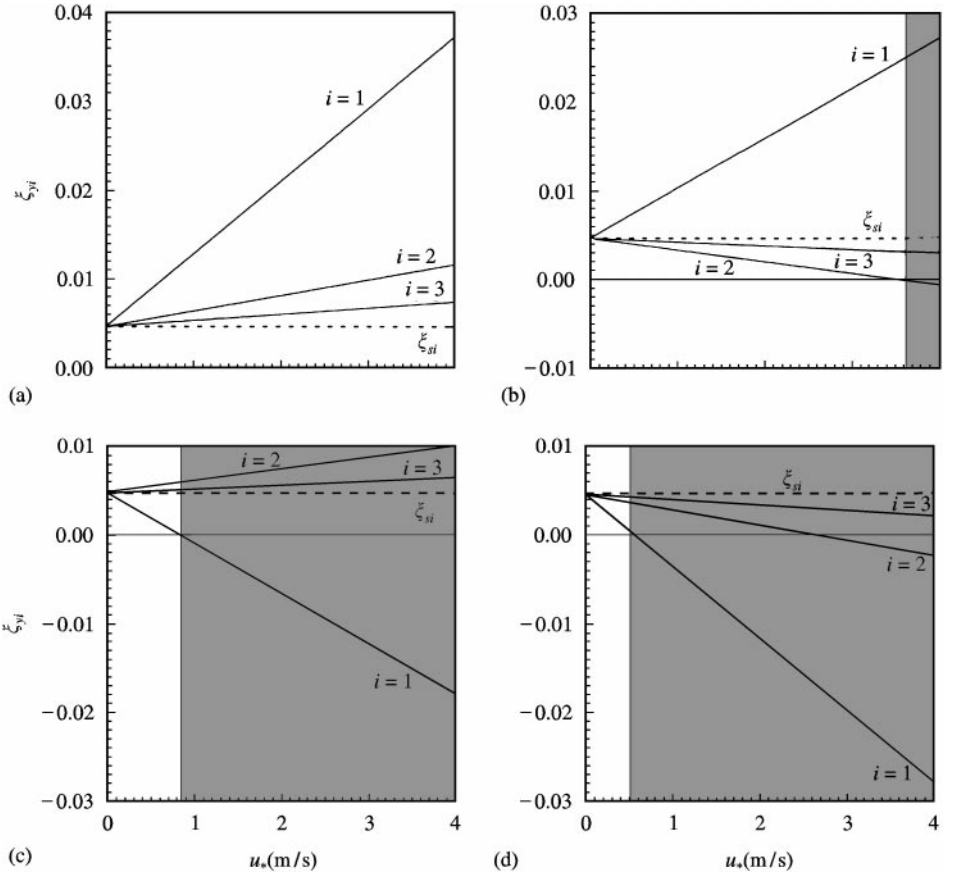

Figure 16. Damping coefficient in the crosswind direction.

modes into account. Dotted lines refer to the solution given by DAWROS using solely the first mode. Dashed lines are related to the gust factor technique applied side by side with the closed-form solution.

DAWROS analyses based on the first mode offer perfect results (solid lines coincide with dotted lines), with the sole exception of the case in which galloping occurs on the second mode (Figure 17b); nevertheless, taking the first two modes into account has no influence on the bifurcation threshold being evaluated correctly. The closed-form solution gives results of increasing precision with increasing u_*. However, due to the hypothesis of near neutral atmospheric conditions, better approximations in the low wind velocity range should be purely illusory.

Figures 18 and 19 show some p.s.d.f.s of the displacement at the top of the shaft close to bifurcation states. Figure 18 corresponds to case B with $u_* = 3{\cdot}2, 3{\cdot}6$ m/s. Figure 19 refers to case C with $u_* = 0{\cdot}4, 0{\cdot}8$ m/s. The ordinate $nS_\alpha(h;n)/\bar{x}^2(h)$ highlights the increase of the resonant peaks of the crosswind response (the second peak in case B, the first peak in case C). Near the bifurcation they overtake the resonant peaks of the alongwind displacement tending to the infinite when, annulling the total damping, galloping occurs.

Figure 20(a) shows the diagrams of the displacement s_1, s_2, s_3 [equation (73)] at the top of the shaft for case A. Since alongwind response always prevails over crosswind response, the

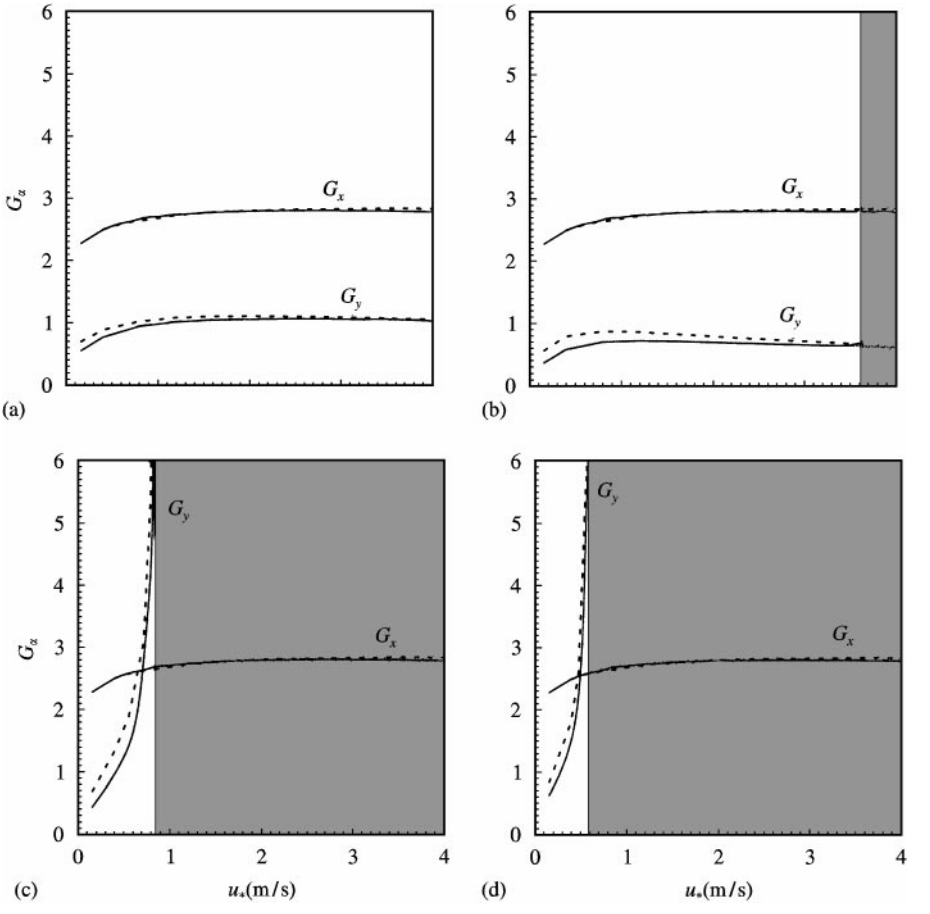

Figure 17. Gust factor for the aerodynamic configurations (a) A; (b) B; (c) C; (d) D in Table 3.

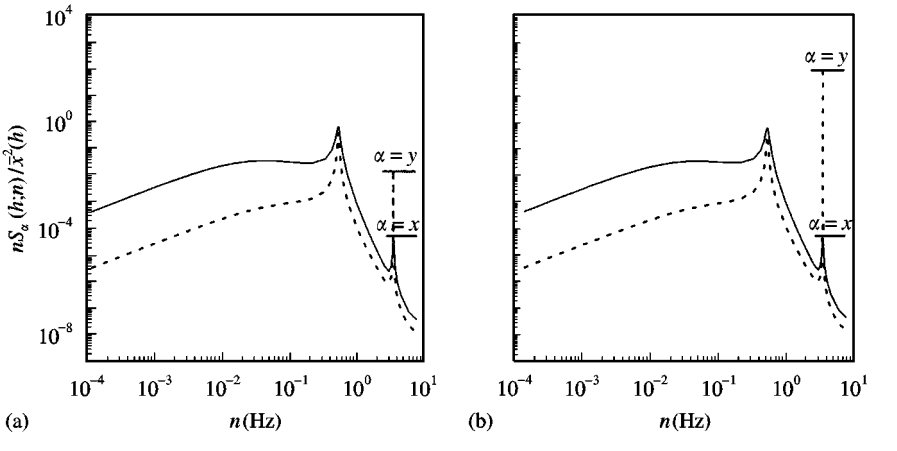

Figure 18. P.s.d.f. of the displacement at the top of the shaft for case B: (a) $u_* = 3{\cdot}2$ m/s; (b) $u_* = 3{\cdot}6$ m/s.

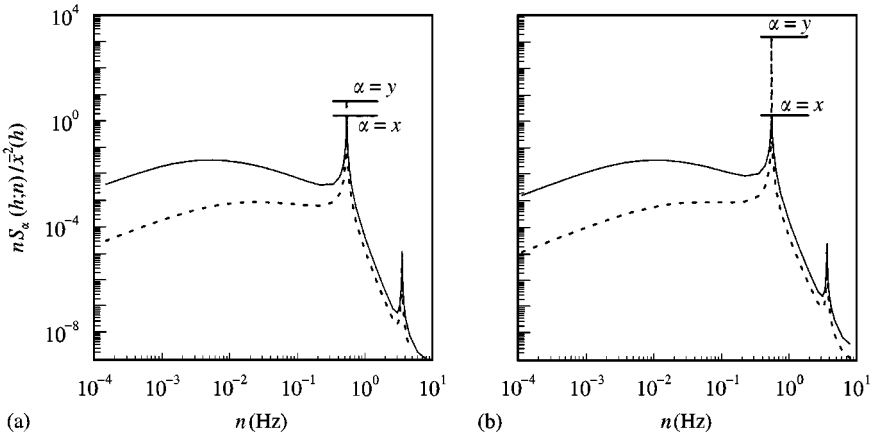

Figure 19. P.s.d.f. of the displacement at the top of the shaft for case C: (a) $u_* = 0{\cdot}4$ m/s; (b) $u_* = 0{\cdot}8$ m/s.

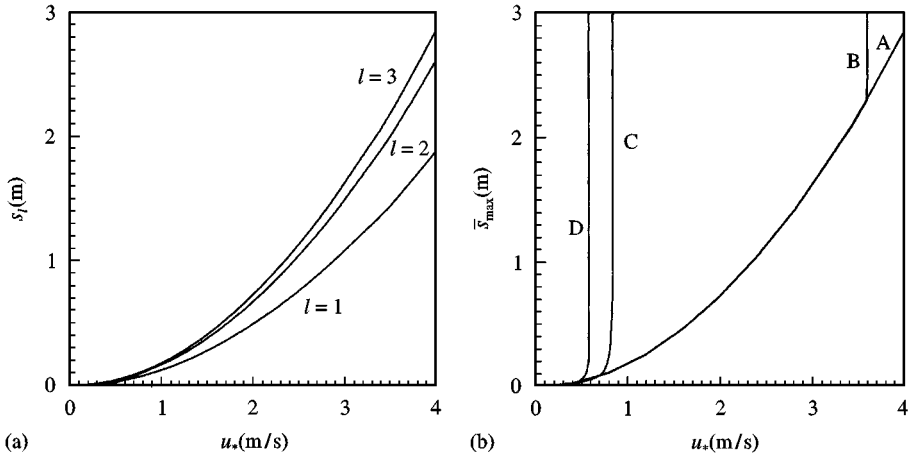

Figure 20. Maximum displacement at the top of the shaft: (a) case A; (b) all cases compared.

maximum value of the displacement is $\bar{s}_{max} = s_3$ [equation (72)]. In cases B, C, D (Figure 20b), close to bifurcation, the crosswind response exceeds the alongwind response and $\bar{s}_{max}$ suddenly passes from s_3 to s_1 (Figure 10). Stresses exhibit analogous properties (Solari & Pagnini 1998).

The knowledge of the actual structural damping points out the role of a suitable evaluation of this parameter. Figure 21 shows the diagrams of the generalized gust factors associated with the aerodynamic configurations previously studied. Dashed lines, derived from Figure 17, correspond to the conventional choice $\xi_{s\alpha i} = 0{\cdot}004775$; solid lines involve the more realistic estimate $\xi_{s\alpha i} = 0{\cdot}01$ (Figure 13); analyses have been carried out in closed form. The bifurcation threshold increases proportionally to structural damping, thus providing a further safety margin especially in correspondence to large energy dissipations. Far from this limit, in the stable regimes, structural damping is dominated by aerodynamic damping and its importance is almost negligible.

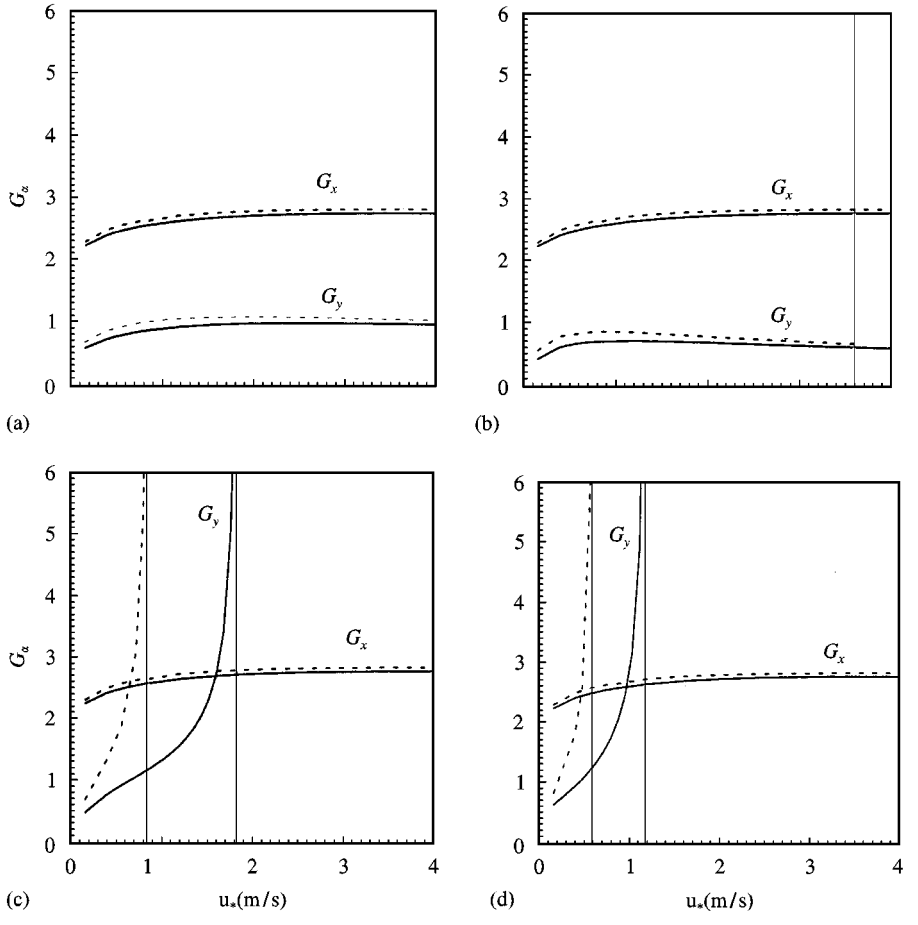

Figure 21. Gust factors for $\xi_{szi} = 0{\cdot}004775$ (dashed lines) and $\xi_{szi} = 0{\cdot}01$ (solid lines): (a) case A; (b) case B; (c) case C; (d) case D.

11. CONCLUSIONS AND PERSPECTIVES

The wind-excited response of poles and monotubular towers represents quite a peculiar problem: on the one hand, it stands at the centre of growing engineering and technological interest; on the other, it allows rather refined analyses consistent with physical reality for this type of structure. The activities coordinated by ACS ACAI Servizi have combined these two aspects, producing an articulated range of studies spreading from experimental and theoretical research to pre-normative, design and production analyses. In this frame of reference, this paper illustrates the formulation of a calculation procedure of the gust buffeting response and galloping instability.

It is shown that a general set-up of this subject, here defined as the first level, leads to analytical developments of extreme complexity both for the bifurcation study of dynamic equilibrium and for the stable response. It suffices to turn to some simple and reasonable approximations, referred to as the second level, for the method to take on such simplified characteristics to allow a solution in closed form. As required by the producers and the designers, this solution is formally analogous to the methods proposed by present codes of practice.

The study points out the central role of structural and aerodynamic damping. Structural damping increases on increasing the motion amplitude, according to laws strictly

depending on the type of structure. Aerodynamic damping is a consequence of aeroelasticity. In the presence of aerodynamically stable shapes, the alongwind response dominates the crosswind response and the masses, above all that at the top, behave as dampers. The presence of aerodynamically unstable shapes, both of the shaft and of the masses, can cause manifold phenomena of potential galloping involving either the first or the second mode. In any case the masses play a major role since, depending on their shape, they either mitigate or exacerbate the oscillations.

Several problems deserving further study come out of this framework. The method so far developed applies the quasi-steady theory taking the longitudinal and lateral turbulence into account. Wind-structure interaction is simulated considering only the alongwind and crosswind displacements. As a matter of fact, due to the large shaft flexibility, the rotations of the local masses in the alongwind and crosswind planes should not be ignored. In this same context, neither vertical turbulence nor moments around the x- and y-axis should be neglected. To overcome these limits the authors are developing a generalized quasi-steady theory for point-like elements (the localized masses) to determine the full aerodynamic forces and aeroelastic properties of steel poles and monotubular towers. It is expected that this formulation may furnish nonclassical aerodynamic actions and damping effects leading to complex galloping conditions. Parallel to this mathematical approach the authors are also planning to carry out wind tunnel tests to determine reliable aerodynamic coefficients including 3-D angular derivatives.

The second aspect which is worth of deeper study concerns the nonlinear behaviour from the mechanical, geometric and aeroelastic viewpoint. Mechanical damping increases with motion amplitude; this means that once the structure takes on a deformation branch leading to bifurcation, the structural motion could be self-limiting because of dissipated energy; it follows that galloping should move towards higher velocities. Such a study requires substantial evolution of both the damping and the response models. From the geometric viewpoint the mass at the summit, paired to large deformation states, brings about second-order effects whose extent must still be investigated. These effects being important, the expansion of the aeroelastic contributions beyond the linear terms is required.

To develop the theory further, the necessity arises to carry out further full-scale tests to validate or calibrate the reliability of models. The authors are about to monitor some poles and monotubular towers to acquire new essential information.

ACKNOWLEDGEMENTS

This research has been carried out with the support of ACS ACAI Servizi. The authors acknowledge the associates of the section *Poles and Monotubular Towers* who cooperated in the project.

References

AIJ Recommendations for Loads on Buildings 1996 Architectural Institute of Japan.

Basis of Design and Actions on Structures 1994 Eurocode 1, Part 2–4: Wind actions, ENV 1991-2-4, European Committee for Standardization.

Characteristics of Atmospheric Turbulence near the Ground. Part II: Single Point Data for Strong Winds (*neutral atmosphere*) 1993 ESDU 85020. London: Engineering Sciences Data Unit.

Damping of Structures. Part I: Tall Buildings 1991 ESDU 83009. London: Engineering Sciences Data Unit.

Lighting Columns 1985 British Standard, BS 5649.

Mean Fluid Forces and Moments on Cylindrical Structures: Polygonal Sections with Rounded Corners Including Elliptical Shapes 1980, ESDU 79026. London: Engineering Sciences Data Unit.

Minimum Design Loads for Buildings and Other Structures 1995 ASCE 7-95. New York: ASCE.
Public Light Poles 1985 European Standard, EN 40/6.
Response of Structures to Atmospheric Turbulence: *Computer Programs A9236 and B9236* 1993, ESDU 92036, London: Engineering Sciences Data Unit.
Structural Standards for Steel Antenna Towers and Antenna Supporting Structures 1991 Electronic Industries Association, Telecommunications Industry Association, EIA/TIA-222-E.
Technical Standards Concerning "General Criteria for Structural Safety and Design Loads" 1996 Ministerial Decree 16th January 1996 (in Italian).
Ballio, G. & Solari, G. 1992 The Park Tower in Milan: a steel structure of 1933 in the light of past and present knowledge. *Costruzioni Metalliche* **3,** 141–164; **4,** 211–233.
Buresti, G. 1998 Vortex shedding from bluff bodies. In *Wind Effects on Buildings and Structures* (eds J. D. Riera & A. G. Davenport), pp. 61–95. Rotterdam: Balkema.
Caughey, T. L. 1960 Classical normal modes in damped linear dynamic systems. *Journal of Applied Mechanics* **27,** 269–271.
Cook, N. J. 1990 *The Designer's Guide to Wind Loading of Buildings. Part 2: Static Structures.* Butterworths: Building Research Establishment.
Davenport, A. G. 1961 The application of statistical concepts to wind loading of structures. *Proceedings of the Institution of Civil Engineers* **19,** 449–472.
Davenport, A. G. 1964 Note on the distribution of the largest value of a random function with application to gust loading. *Proceedings of the Institution of Civil Engineers* **24,** 187–196.
Den Hartog, J. P. 1932 Transmission line vibration due to sleet. *AIEE Transactions* **51,** 1074–1076.
Elishakoff, I. 1983 *Probabilistic Methods in the Theory of Structures.* New York: Wiley.
Hallam, M. G., Heaf, N. J. & Wootton, L. R. 1978 Dynamics of marine structures: methods of calculating the dynamic response of fixed structures subject to wave and current action. CIRIA Report UR 8.
Holmes, J. D., Schafer, B. L. & Banks, R. W. 1992 Wind-induced vibration of a large broadcasting tower. *Journal of Wind Engineering and Industrial Aerodynamics* **41–44,** 2101–2110.
Holscher, N. & Niemann, H. J. 1996 Turbulence and separation induced pressure fluctuations on a finite circular cylinder — application of a linear unsteady strip theory. *Journal of Wind Engineering and Industrial Aerodynamics* **65,** 335–346.
Hurty, W. C. & Rubinstein, M. F. 1964 *Dynamics of Structures.* Englewood Cliffs: Prentice-Hall.
Jones, K. F. (1992) Coupled vertical and horizontal galloping. *ASCE Journal of Structural Engineering* **118,** 92–107.
Kawai, H. 1983 Pressure fluctuations on square prisms — applicability of strip and quasi-steady theories. *Journal of Wind Engineering and Industrial Aerodynamics* **13,** 197–208.
Meirovitch, L. 1980 *Computational Methods in Structural Dynamics.* Alphen aan den Rijn: Sijthoff & Noordhoff.
Pagnini, L. C., Lagomarsino, S. & Solari, G. 1999 Experimental evaluation of damping of poles and monotubular towers. *Costruzioni Metalliche* **1,** 39–51 (in Italian).
Piccardo, G. & Luongo, A. 1995 Stability critical conditions for coupled flexural galloping. *Proceedings of the Twelfth National Conference of Theoretical and Applied Mechanics*, *AIMETA*, pp. 161–166, Napoli (in Italian).
Piccardo, G. & Solari, G. 1996 A refined model for calculating 3-D equivalent static wind forces on structures. *Journal of Wind Engineering and Industrial Aerodynamics* **65,** 21–30.
Piccardo, G. & Solari, G. 1998a Generalized equivalent spectrum technique. *Wind and Structures* **1,** 161–174.
Piccardo, G. & Solari, G. 1998b 3-D wind-excited response of slender structures: basic formulation, closed form solution, applications. *ASCE Journal of Structural Engineering*, accepted for publication.
Piccardo, G. & Solari, G. 1998c Closed form prediction of the 3-D wind-excited response of slender structures. *Journal of Wind Engineering and Industrial Aerodynamics* **74–76,** 697–708.
Simiu, E. 1973 Logarithmic profiles and design wind velocities. *ASCE Journal of Engineering Mechanics* **99,** 1073–1083.
Simiu, E. & Lozier, D. W. 1979 The buffeting of tall structures by strong winds — Windload program. NTIS Accession PB294757/AS. Springfield: National Technical Information Service.
Simiu, E. & Scanlan, R. H. 1996 *Wind Effects on Structures.* New York: Wiley.
Solari, G. 1981 DAWROS: A computer program for calculating the Dynamic Along-Wind Response Of Structures. Istituto di Scienza delle Costruzioni, University of Genova, Series IV, 1.

Solari, G. 1982 Alongwind response estimation: closed form solution. *ASCE Journal of the Structural Division* **108,** 225–244.
Solari, G. 1987 Turbulence modeling for gust loading. *ASCE Journal of Structural Engineering* **113,** 1550–1569.
Solari, G. 1988 Equivalent wind spectrum technique: Theory and applications. *ASCE Journal of Structural Engineering* **114,** 1303–1323.
Solari, G. 1992 Wind actions and effects on urban light poles. Unpublished report.
Solari, G. 1993a Gust buffeting. I: peak wind velocity and equivalent pressure. *ASCE Journal of Structural Engineering* **119,** 365–382.
Solari, G. 1993b Gust buffeting. II: dynamic alongwind response. *ASCE Journal of Structural Engineering* **119,** 383–398.
Solari, G. 1994 Gust-excited vibrations. In *Wind-Excited Vibrations of Structures* (ed. H. Sockel), pp. 195–291. Wien: Springer Verlag.
Solari, G. & Pagnini, L. C. 1998 The actions and effects of wind on poles and monotubular towers. *Costruzioni Metalliche* **4,** 29–51 (in Italian).
Solari, G. & Piccardo, G. 1999. Probabilistic 3-D turbulence modeling for gust buffeting. *Probabilistic Engineering Mechanics*, accepted for publication.
Solari, G., Reinhold, T. A. & Livesey, F. 1998 Investigation of wind actions and effects on the Leaning Tower of Pisa. *Wind and Structures* **1,** 1–25.
Yam, L. H., Leung, T. P., Li D. B. & Xue, K. Z. 1997 Use of ambient response measurements to determine dynamic characteristics of slender structures. *Engineering Structures* **19,** 145–152.